European Journal of Medicinal Chemistry 67 (2013) 127–141

Contents lists available at SciVerse ScienceDirect

European Journal of Medicinal Chemistry

journal homepage: http://www.elsevier.com/locate/ejmech

Original article

# Phosphanegold(I) dithiocarbamates, $R_3PAu[SC(=S)N(^iPr)CH_2CH_2OH]$ for R = Ph, Cy and Et: Role of phosphane-bound R substituents upon in vitro cytotoxicity against MCF-7R breast cancer cells and cell death pathways

Nazzatush Shimar Jamaludin [a], Zheng-Jie Goh [b], Yoke Kqueen Cheah [b,**], Kok-Pian Ang [b], Jiun Horng Sim [b], Chai Hoon Khoo [b], Zainal Abidin Fairuz [a], Siti Nadiah Binti Abdul Halim [a], Seik Weng Ng [a,c], Hoi-Ling Seng [a], Edward R.T. Tiekink [a,*]

[a] Department of Chemistry, University of Malaya, 50603 Kuala Lumpur, Malaysia
[b] Department of Biomedical Science, Faculty of Medicine and Health Sciences, Universiti Putra Malaysia, 43400 Serdang, Malaysia
[c] Chemistry Department, Faculty of Science, King Abdulaziz University, P.O. Box 80203, Jeddah, Saudi Arabia

ARTICLE INFO

*Article history:*
Received 19 March 2013
Received in revised form
11 June 2013
Accepted 13 June 2013
Available online 26 June 2013

*Keywords:*
Gold(I) complexes
Dithiocarbamate
Cancer
Chrysotherapy
Cell cycle
Metallopharmaceuticals

ABSTRACT

The synthesis and characterisation of $R_3PAu[S_2CN(^iPr)CH_2CH_2OH]$, for R = Ph (**1**), Cy (**2**) and Et (**3**)4, is reported. Compounds **1**–**3** are cytotoxic against the doxorubicin-resistant breast cancer cell line, MCF-7R, with **1** exhibiting greater potency and cytotoxicity than either of doxorubicin and cisplatin. Based on human apoptosis PCR-array analysis, caspase activities, DNA fragmentation, cell apoptotic assays, intracellular reactive oxygen species (ROS) measurements and human topoisomerase I inhibition, induction of apoptosis by **1**, and necrosis by **2** and **3**, are demonstrated, by both extrinsic and intrinsic pathways. Compound **1** activates the p53 gene, **2** activates only the p73 gene, whereas **3** activates both the p53 and p73 genes. Compounds **1** and **3** activate NF-κB, and each inhibits topoisomerase I.



## 1. Introduction

Dithiocarbamate derivatives, such as diethyldithiocarbamate [$^-S_2CNEt_2$], are well known to exhibit useful pharmacological properties. For example, they inhibit superoxide dismutase (SOD) [1] and reduce alkylation of DNA by nitrosoamines [2]. Owing to their strong chelating ability towards metals, they have long been used in the treatment of Wilsons disease where they facilitate the removal of excess copper [3], and reduce nephrotoxicity associated with cisplatin therapy [4]. Metal complexes of dithiocarbamates also offer opportunities as therapeutics [5], exhibiting potential as anti-microbial, anti-viral, anti-cancer, etc. agents. In relation to the latter, several metal dithiocarbamate show promise, ranging from main group elements, tin [6] and bismuth [7], to transition metals, such as zinc [8], copper [9] and gold [10]. Gold dithiocarbamate complexes in particular display great potential and are one of the key classes of compound behind the resurgence of investigations of gold(III) compounds as anti-cancer drugs [11,12]. Thus, early work on in vitro cytotoxicity profiles exhibited by phosphanegold(I) dithiocarbamates [13] was rapidly surpassed by investigations into the efficacy and possible mechanisms of action exhibited by gold(III) dithiocarbamates [14–17]. In continuation of studies into the anti-cancer potential of phosphanegold(I) thiolates, herein the cytotoxicity and mechanisms of cell death against MCF-7R breast cancer cells for a series of triorganophosphanegold(I) dithiocarbamates, $R_3PAu[S_2CN(^iPr)CH_2CH_2OH]$ for R = Ph (**1**), Cy (**2**) and Et (**3**), Scheme 1, bearing hydrophilic ethanol substituents, are reported.

Mitigating curative therapy of advanced breast cancer is the development of anti-cancer drug resistance. Despite mammary

* Corresponding author. Tel.: +60 3 7967 6775; fax: +60 3 7967 4193.
** Corresponding author.
*E-mail addresses:* yokekqueen@gmail.com (Y.K. Cheah), Edward.Tiekink@um.edu.my, edward.tiekink@gmail.com (E.R.T. Tiekink).

0223-5234/$ – see front matter © 2013 Elsevier Masson SAS. All rights reserved.
http://dx.doi.org/10.1016/j.ejmech.2013.06.038

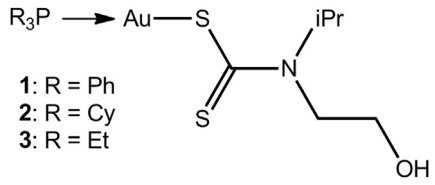


**Scheme 1.** Chemical structures of the investigated triorganophosphinegold(I) dithiocarbamates.

carcinomas being considered as one of the most chemosensitive solid tumours, most initially responsive tumours relapse, develop resistance to a broad spectrum of drugs and in metastatic patients, treatment failure occurs frequently. Thus, breast cancer becomes refractory to anti-cancer drugs and is therefore often incurable [18,19]. For metastatic cancers, it is estimated that drug resistance causes failure in over 90% of patients under-going treatment [20,21]. There are a variety of mechanisms by which tumours become resistant to chemotherapy, including alteration in cell cycle checkpoints, breakdown in apoptotic mechanisms, enhanced drug efflux as well as altered DNA repair and scavenging enzymes [22–24]. In cases where simultaneous resistance of tumours to a number of structurally and functionally unrelated chemotherapeutic agents is termed Multi-Drug Resistance (MDR) [25]. One of the most extensively studied mechanisms of MDR relates to the over-expression of transmembrane P-glycoprotein (P-gp), that functions as a drug efflux pump to reduce the intracellular concentration of drugs and, thus, cytotoxic activity [24,26].

The anti-cancer drug, doxorubicin, an anthracycline anti-biotic produced by the fungus *Streptomyces peucetius* [27], is widely used in the treatment of leukaemia, breast carcinoma and other solid tumours [28]. However, response rates to single doxorubicin treatment range from 43% in previously untreated patients to 28% in patients previously exposed to the drug [29], an observation which indicates that growing resistance to doxorubicin can lead to an unsuccessful outcome in nearly 50% of treated patients, making resistance a major cause of treatment failure.

In line with the foregoing, in spite of the development of new targeted and effective anti-cancer therapies, mechanisms that evolve to protect cancer cells against these chemotherapeutic agents will continue to act as serious obstacles to the successful treatment of cancer. Hence, the development of new anti-cancer agents, especially with novel mechanisms of activity, will lead to better treatment regimes for cancer patients. In consideration of this, in the present study the cytotoxic activities of compounds **1**–**3** were evaluated against the doxorubicin-resistant variant of human breast adenocarcinoma cell line, MCF-7R. In addition, in order to determine cell death mechanisms, DNA fragmentation, caspase detection, intracellular reactive oxygen species (ROS) measurements, membrane permeability, human topoisomerase I inhibition assay and real-time quantification of gene expression by employing the polymerase chain reaction array technology ($RT^2$ Profiler™ PCR Array) were performed.

## 2. Results and discussion

### 2.1. Synthesis and spectroscopic characterisation

Compounds **1**–**3** were readily prepared in good yields by the metathetical reaction between the respective $R_3PAuCl$ precursor and $Na[S_2CN(^iPr)CH_2CH_2OH]$. The compounds are air- and light-stable solids, soluble in acetone, chloroform and DMSO, and have been characterised by various spectroscopic methods, e.g., multi-nuclear NMR and IR, to reveal the expected characteristics detailed in Section 4.2. As it was possible to obtain crystals for **2** and **3**, their unambiguous structure determination was achieved using X-ray crystallography.

### 2.2. X-ray crystallography

The molecular structure of **2** is shown in Fig. 1. Selected geometric bond lengths (Å) and angles (°) for **2** and for **3** are collected in Table 1. The gold atom exists within a linear donor set defined by the phosphane-P1 and dithiocarbamate-S1 atom. The Au–S1 bond length is considerably longer than the Au–P1 bond and the deviation from the ideal 180° angle at gold can be ascribed to the presence of a close intramolecular Au···S2 contact of 3.0386(9) Å. The monodentate mode of coordination of the dithiocarbamate ligand is reflected in the disparity in the C–S bond lengths with the shortest of these being associated with the weakly binding S2 atom, Table 1. A very similar structure is found for the triethylphosphane analogue, **3**. In this case, Fig. 2, the crystallographic asymmetric unit comprises two independent molecules and, as can be seen from the overlay diagram in Fig. 3, there are only minor conformational changes between them. It is interesting to correlate the magnitude of the intramolecular Au···S2 interactions with the deviations from linearity of the P–Au–S bond. In **3**, where the Au···S2 interactions are longer, the deviations from the ideal 180° are reduced. The overlay diagram, Fig. 3, also includes the skeletal structure of **2** and serves to highlight the similarity in the molecular structures of **2** and **3**. The molecular structure of **2** closely resembles literature precedents [30,31], and in the same way **3** matches a literature structure [32]. In fact, all mentioned structures match the original structure determination reported for $Ph_3PAu(S_2CNEt_2)$ [33], and on this basis, it is anticipated that the molecular structure of **1**, for which crystals could not be obtained, despite repeated attempts, follows the same trends as described above.

Each of **2** and **3** features hydroxyl groups in the dithiocarbamate anion and these form significant hydrogen bonding interactions in their respective crystal structures. In **2**, a supramolecular helical chain along the *b*-axis (Fig. S1) is formed via O–H···S hydrogen bonds involving the non-coordinating S2 atom. A similar aggregation mode is found for each of the independent molecules in **3** where Au1-containing molecules self-associate into a helical chain along the *b*-axis via O–H···S hydrogen bonds, Fig. 4; the same occurs for the Au2-containing molecules (Fig. S2). Consistent with the steric bulk of the cyclohexylphosphane ligands, supramolecular chains of **2** pack in the crystal structure with no specific intermolecular interactions between them (Fig. S3). By contrast, chains of **3**

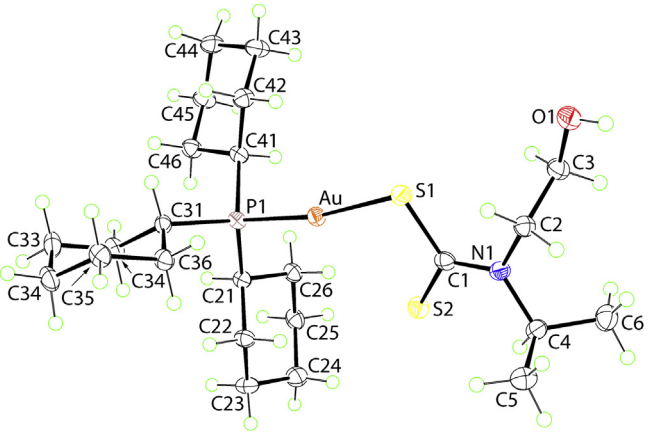


**Fig. 1.** The molecular structure of **2**, showing atom-labelling scheme.

**Table 1**
Selected geometric parameters (Å, °) for **2** and **3**.[a]

| Compound | **2** | **3** (Molecule 1) | **3** (Molecule 2)[a] |
|---|---|---|---|
| *Parameter* | | | |
| Au–S1 | 2.3442(8) | 2.3380(19) | 2.3347(19) |
| Au–P1 | 2.2648(8) | 2.2529(19) | 2.255(2) |
| Au···S2 | 3.0386(9) | 3.112(2) | 3.112(2) |
| C1–S1, S2 | 1.751(3), 1.697(3) | 1.745(6), 1.725(7) | 1.749(7), 1.713(7) |
| C1–N1 | 1.346(4) | 1.333(8) | 1.340(9) |
| S1–Au–P1 | 170.79(3) | 176.22(7) | 174.68(6) |
| Au–S1–C1 | 98.21(11) | 99.1(2) | 99.6(2) |

[a] For atom labels add 10.

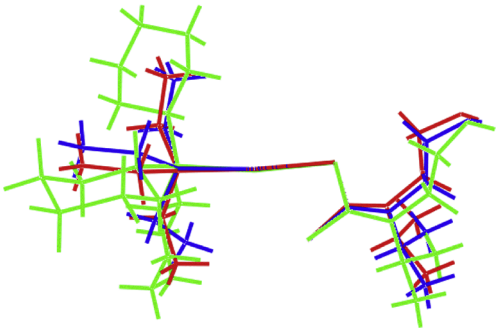

**Fig. 3.** Overlay diagram of the two independent molecules, Au1 (red image) and Au11 (blue), comprising the asymmetric unit of **2**, and of **3** (green). The molecules have been superimposed so that the $AuS_2$ residues are coincident. (For interpretation of the references to colour in this figure legend, the reader is referred to the web version of this article.)

associate into a three-dimensional architecture via C–H···O/S interactions (Fig. S4).

### 2.3. Inhibition of MCF-7R breast cancer cell proliferation

Compounds **1**–**3** were evaluated in vitro by testing for inhibition of cell proliferation against a doxorubicin-resistant variant of human breast carcinoma cell lines (MCF-7R), using Na[$S_2CN(^iPr)CH_2CH_2OH$] (**4**), doxorubicin and cisplatin as the positive controls. The effects of the six compounds on the growth of MCF-7R were evaluated after 24 h and the obtained $IC_{50}$ values are listed in Table 2. From these data it can be seen that **1**–**3** each promoted significant inhibition of cell proliferation and potency levels comparable or greater than exhibited by cisplatin; Na[$S_2CN(^iPr)CH_2CH_2OH$] was non-cytotoxic. Compound **1** was the most active among the series, exhibiting potency about 4.5 times that of cisplatin and displays a smaller $IC_{50}$ than doxorubicin under similar experimental conditions; compounds **2** and **3** were less potent than doxorubicin. The viability of the MCF-7R cells after treatment with **1**–**4** at different concentrations is plotted in Fig. 5. Exposure to increasing concentrations of **1**–**3** resulted in a significant dose-dependent inhibition of cell proliferation. This cell mortality was triggered by apoptotic processes characterised by chromatin condensation and DNA fragmentation, as discussed below.

The above results are based on trials conducted in triplicate. Similarly, the observations discussed in Sections 2.4–2.7 are based on experiments performed in triplicate.

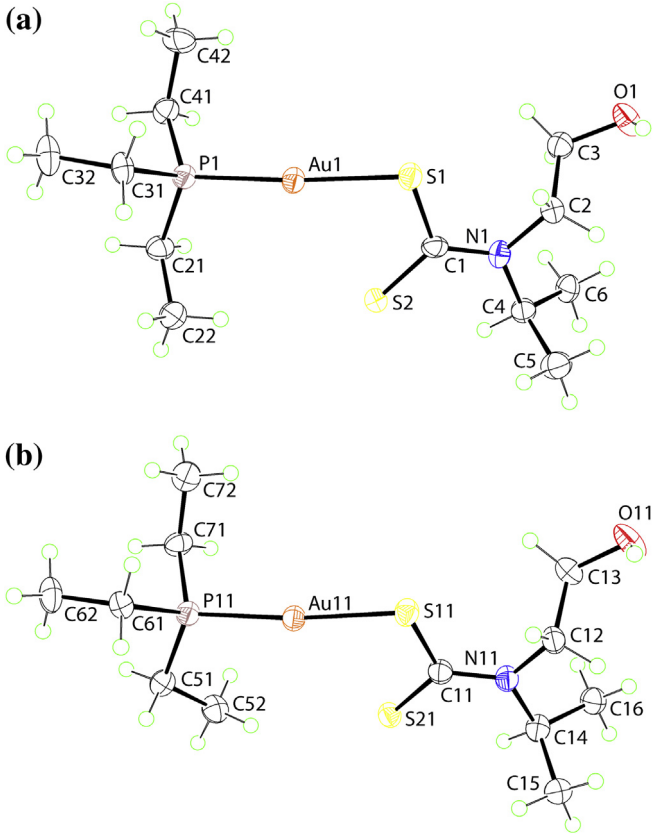


**Fig. 2.** (a) and (b) The molecular structures of the two independent molecules comprising the asymmetric unit of **3**, showing atom-labelling scheme.

### 2.4. Membrane permeability study (AO/PI apoptotic cell study)

The MCF-7R cells were treated with each of **1**–**3**, at the respective $IC_{50}$ dose and then stained with AO/PI in order to evaluate the membrane integrity, Fig. 6. It is known that apoptotic

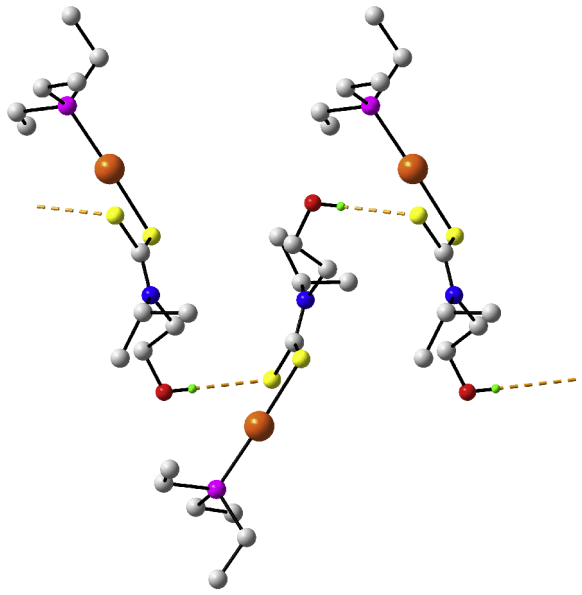

**Fig. 4.** A view of the helical supramolecular chain along the *b*-axis formed by the Au1-containing molecule and sustained by O–H···S2 [OH···$S2^i$ = 2.46 Å; O1···$S2^i$ = 3.282(6) Å; angle at H = 164° for symmetry operation i: $1 - x, -½ + y, -z$] hydrogen bonds, shown as orange dashed lines, in **3**. Hydrogen atoms not participating in hydrogen bonding are omitted for clarity. (For interpretation of the references to colour in this figure legend, the reader is referred to the web version of this article.)

**Table 2**
Cytotoxic activities of **1**–**3**, Na[$S_2CN(^iPr)CH_2CH_2OH$] (**4**), doxorubicin and cisplatin against the MCF-7R cancer cell model after 24 h treatment.[a]

| Compound | $IC_{50}$ (μM) |
|---|---|
| **1** | 4.4 ± 0.4 |
| **2** | 13.6 ± 0.2 |
| **3** | 9.3 ± 0.3 |
| **4** | >80 |
| Doxorubicin | 5.1 ± 0.2 |
| Cisplatin | 19.6 ± 0.4 |

[a] Means and standard deviation of at least two independent experiments conducted in triplicate; not for **4** which was non-cytotoxic.

cells exhibit increased plasma membrane permeability to certain fluorescent dyes [34]. Thus, the membrane-permeable, monovalent and cationic dye, Acridine Orange (AO), binds to nucleic acids. In cells, a low concentration of AO causes a green fluorescence, while at high concentrations a red fluorescence is apparent [35]. When viewed by fluorescence microscopy, cells with an intact membrane appear to have a plain bright-green nucleus while apoptotic cells exhibit a bright-green nucleus with additional features within (apparent as dense-green areas) due to the condensation of chromatin; representative cells are highlighted by arrows in Fig. 6(a) (right-hand image). On the other hand, Propidium Iodide (PI) is impermeable to plasma membranes, but it easily penetrates the plasma membrane of dead or dying cells by intercalating in DNA or RNA, producing bright-red fluorescence [36]. Therefore, cells that have lost membrane integrity will show red staining throughout the cytoplasm and a halo of green staining on the cell surface (plasma membrane). Apoptosis can be characterised by nuclear condensation with cytoplasm alteration and nuclear fragmentation [37]. In the present study, the AO/PI staining showed that majority of MCF-7R cells underwent apoptosis after treatment with **1**, Fig. 6(b), whereas only small portion of apoptotic cells was observed after treatment with **2** and **3** (Fig. 6(c) and (d)). The morphological characteristics include condensation of nuclear chromatin and cytoplasm, membrane blobbing and the formation of apoptotic bodies. The apoptotic bodies appear to be round or oval masses of cytoplasm, and smaller than the size of the cell of origin. By contrast to cells treated with **1**, a large amount of necrotic cells was observed after treatment with **2** and **3** (Fig. 6(c) and (d)), especially after treatment with **2**, where about 70% of MCF-7R cells underwent cell necrosis. Interestingly, some of the **1**- and **3**-treated cells exhibited enlargement of cell volume and formation of multinucleated cells. Further, most of the cells were clumped together in a few colonies (Fig. 6(b), (c) and (d)); this phenomenon was not apparent for the cells treated with doxorubicin. The control cells appeared to be shiny, clear and healthy but a small number of necrotic cells with ruptured plasma membrane were observed (Fig. 6(e)). Finally, the number of apoptotic cells for the **1**-treated cells was significantly greater than doxorubicin-treated cells.

### *2.5. Determination of mode of cell death (DNA fragmentation study)*

One of the hallmarks of the terminal stages of apoptosis is the fragmentation of chromosomal DNA that proceeds in a two-step manner: the DNA is initially cleaved into 50–300 kb fragments and eventually into oligonucleosomal pieces [38,39]. In this study, confirmation of apoptosis-induced cell death of MCF-7R cells after exposure to **1**–**3** is presented in Fig. 7 which shows DNA ladder fragmentation.

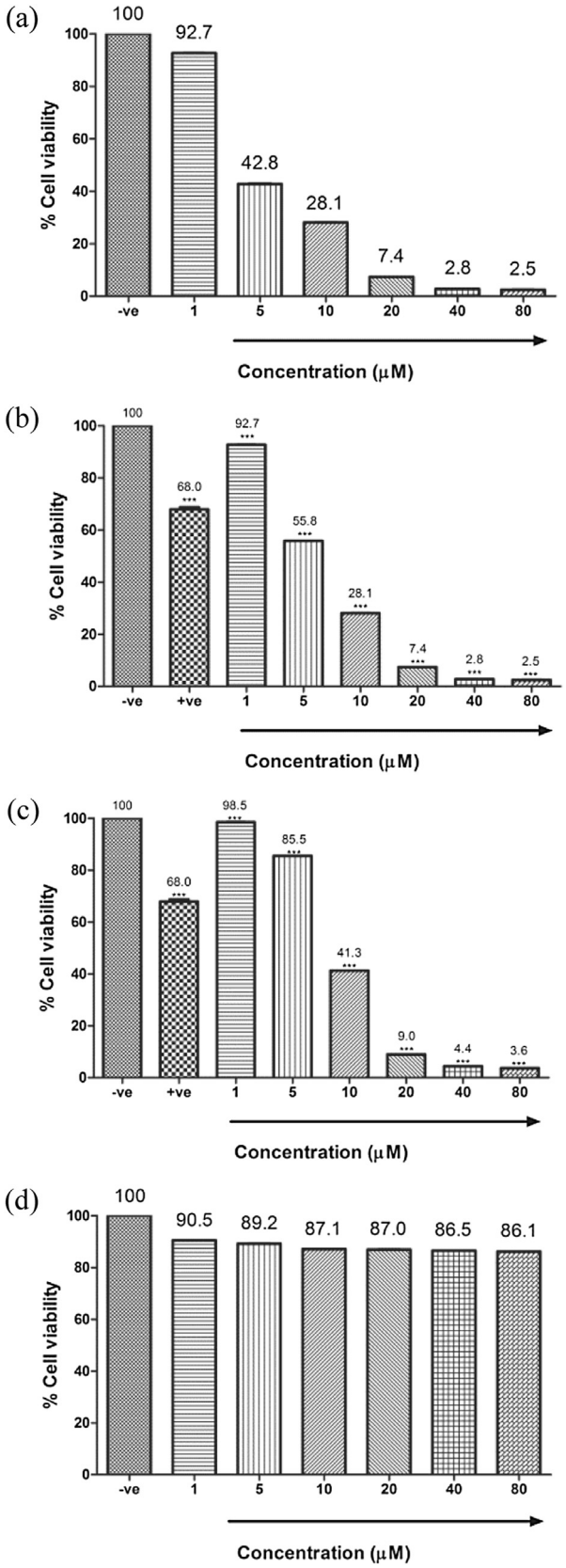


**Fig. 5.** MCF-7R cell viability after treatment of (a) **1**, (b) **2**, (c) **3** and (d) **4** at different concentrations (μM). *P* value = 0.005 in each case.

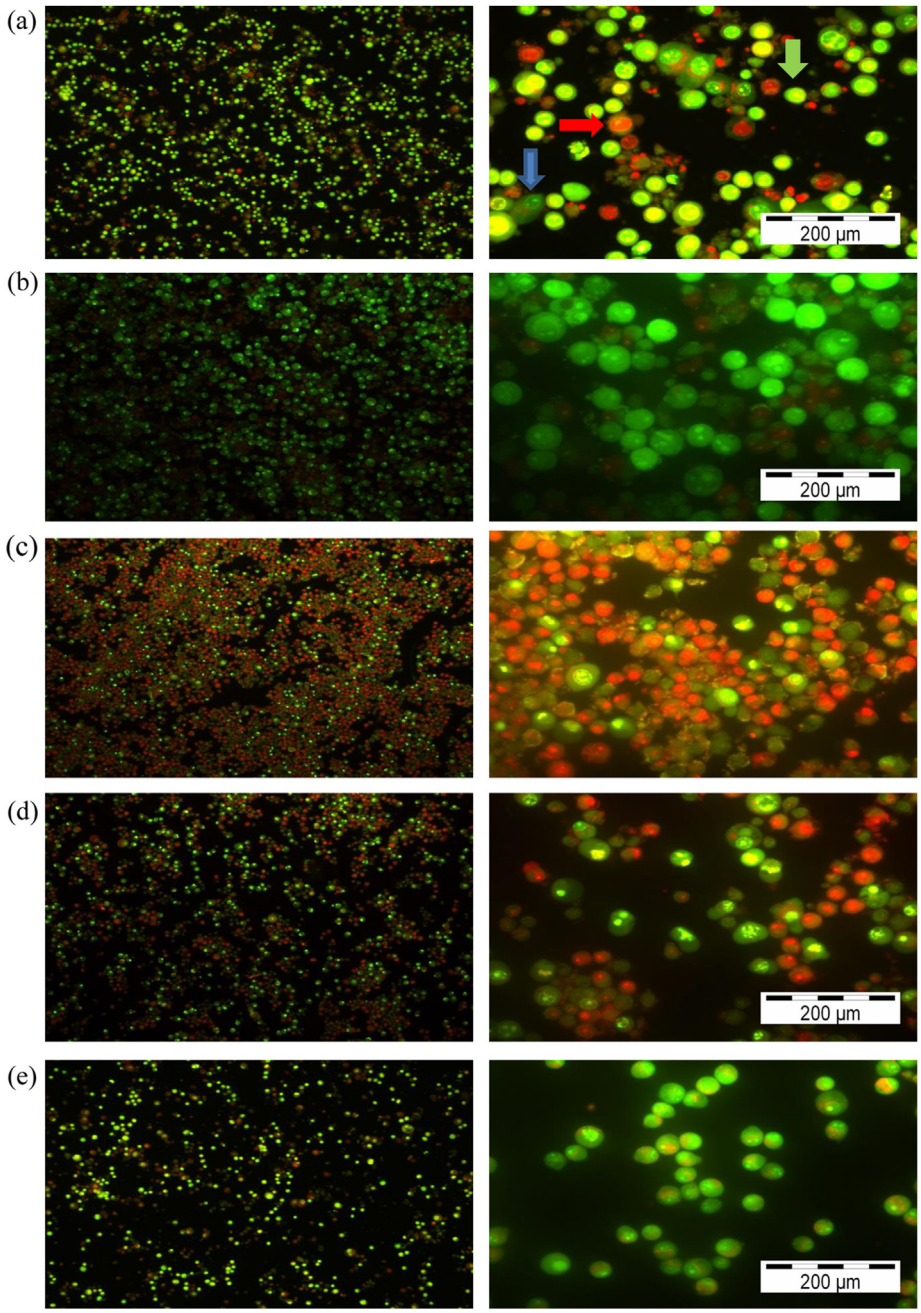


**Fig. 6.** AO/PI staining of MCF-7R cells after being treated at the $IC_{50}$ value of each compound: (a) treated with doxorubicin; (b) treated with **1**; (c) treated with **2**; (d) treated with **3**; (e) untreated cells (negative control). The red colour was produced by PI staining which penetrated the nuclear matter when the cell membrane integrity was disturbed. Cells with intact membrane are stained green. Apoptotic cells are stained green with nuclei stained red, and contain multiple yellow/green dots of condensed nuclei. Necrotic cells were stained bright-red owing to the influx of PI stain. In (a), the green arrow points to a healthy cell, the red arrow shows a necrotic cell, and the blue arrow shows an apoptotic cell with fragmented nucleus and condensed chromatin. Magnification = 100×. (For interpretation of the references to colour in this figure legend, the reader is referred to the web version of this article.)

### *2.6. Analysis of apoptotic pathway (PCR array study and caspase activity)*

In this section an analysis of the PCR array study is made to ascertain the pathways leading to cell death. The up- or down-regulation of genes indicated in this study is correlated with other indicators such as caspase activities.

There are two recognised cellular processes that result in the death of cells, cell necrosis and programmed cell death (PCD) or apoptosis. Cell necrosis is usually triggered by extrinsic factors such as direct physical injury, acute changes in environmental conditions and pathogenic activity, and results in a collapse of cell integrity. The insult will often concurrently affect many cells within a tissue [40,41]. Caspases are crucial for cell apoptosis and are known to operate both through the receptor-mediated pathway, containing members of the tumour necrosis factor (TNF) family of death receptors, and the mitochondrial-mediated pathway, involving cytochrome c release from the mitochondria [42].

In this study, investigations into the in vitro mechanisms of **1**–**3**-induced MCF-7R cell death have been conducted. As discussed below, the results clearly indicate that the gold compounds trigger different levels of anti/pro-apoptotic gene expression. Further, this

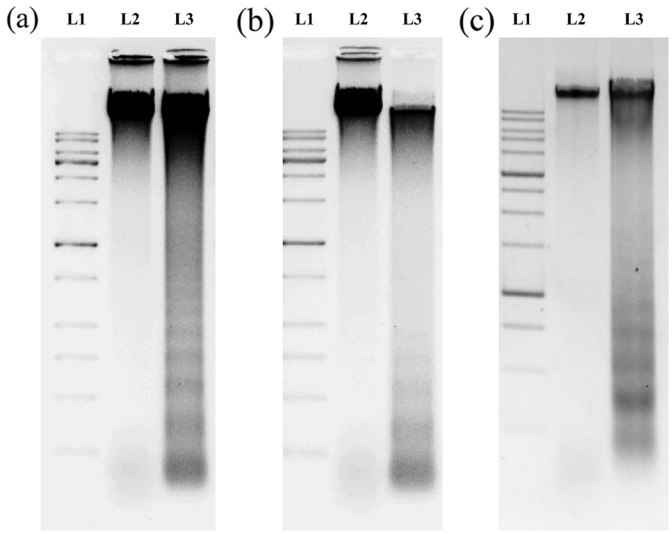


**Fig. 7.** DNA fragmentation analysis. The MCF-7R cells were cultured for 24 h in RPMI 1640 control media in the presence of 4.4 μM **1** ((a) L3), 13.6 μM **2** ((b) L3) and 9.3 μM **3** ((c) L3). DNA was extracted from the cultures and DNA fragmentation was detected using an electrophoresis system with 2% agarose gel. L1 (a)–(c) are 1 kb DNA ladder, and L2 (a)–(c) is the negative control (untreated cells). Formation of ladders on the gels to indicate DNA fragmentation occurs following treatment with **1**–**3** supports cell death by apoptosis.

work provides evidence that the cytotoxicity of **1**–**3** is related to the induction of a p53/p73-dependent activation of the mitochondrial pathway of apoptosis, demonstrating the anti-cancer potential of **1**–**3**. Interestingly, the apoptosis PCR array analysis demonstrated that **1**–**3**-induced apoptosis involved both intrinsic and extrinsic pathways mediated by different kinds of apoptosis-inducing factors. The three different apoptotic pathways induced by **1**–**3** are summarised in Fig. 8.

While in general, **1**–**3** possess a similar apoptotic pathway in which p53/p73 is activated when DNA repair systems are overburdened due to excessive DNA damage, different mechanisms are evident, dependent on the phosphane-bound R group. The p53/p73 genes also act as an upstream inducer of apoptosis by activating the expression of genes encoding either MMP-inducing proteins of the BCL-2 family, such as BAX, BID, NOXA and PUMA, or other apoptotic and cell cycle regulators [43–45]. The up-regulation of the p53/p73 genes indicates that **1**–**3** could induce DNA damage in MCF-7R cells and is consistent with the DNA fragmentation results discussed above (Fig. 7). Curiously, each of **1**–**3** expressed p53 and p73 to different extents. Thus, both p53 and p73 were expressed when treatment was with **3**. On the other hand, gene expression of only p53 and its binding protein were found when treatment was with **1**. Finally, **2** was found to trigger the gene expression of p73 only, as seen by about a 3200-fold greater increase in TP73 expression compared to the untreated control cells (Table 3). Besides that, the presence of c-Abl assures the enhancement of p73-induced apoptosis after treatment of **2** and **3**, therefore the subsequent redistribution of p73 might well occur in the onset of apoptosis [46]. Moreover, the high expression of the BNIP3L gene, a cell death inducer, in **1**- and **3**-treatment (37.23- and 29.33-fold, respectively) is supportive evidence for the activation of the p53 gene. Generally, p53 can directly up-regulate expression of BNIP3L, which is known to be highly induced in wild-type p53-expressing cells, due in part, to sequestering of p53 and CBP (CREB-binding protein) to BNIP3L during hypoxia [47].

With respect to DNA damage, p73 has been reported to be involved in the cellular response. When over-expressed in cells, it could activate the transcription of p53-responsive genes such as $p21^{WAF1}$, Bax, Mdm2, and GADD45, and inhibit cell growth in a p53-like manner by inducing apoptosis [48]. In contrast to the p53 gene, mutations of p73 are rarely found in most human cancers [49,50]. In the main this dangerous protein is inactive as, under normal conditions, steady-state expression levels of endogenous p73 are maintained at an extremely low level. However, p73 is induced in response to a subset of genotoxic stresses, such as by treatment with the oncotoxic drug cisplatin and ionising radiation, and accumulates in proteins, resulting in either G1/S cell cycle arrest or commitment to death through apoptosis [51]. It is now well established that p73 expression is clearly involved in tumourigenesis and is activated in response to chemotherapy [52]. This is of particular importance, since p73 is rarely mutated in cancer cells (less than 0.5%), as compared to p53 (over 50%).

A second mechanism of p53/p73-induced apoptosis is mediated by induction of BAX and BCL-2-associated X protein, which in turn promotes Bax mitochondrial translocation and cytochrome c

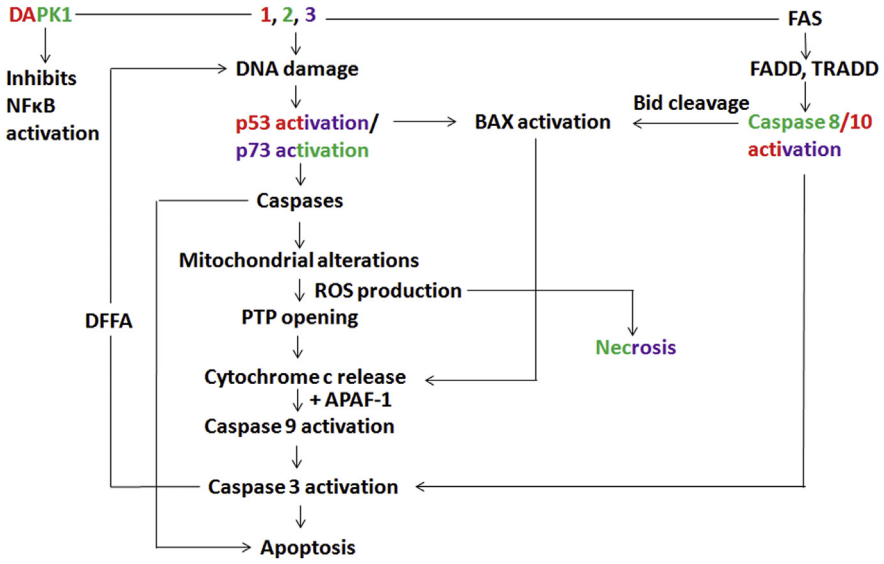


**Fig. 8.** Signalling pathway of apoptosis induced by **1**, **2** and **3**. This diagram collates and summarises the results of the PCR array analysis, caspase activity study, DNA fragmentation and ROS production measurements.

**Table 3**
Effects of **1**–**3** on apoptosis-related gene expression in MCF-7R cancer cells.[a]

| | Up-Down Regulation Fold Regulation (comparing to control group) | | | | Fold Regulation (comparing to control group) | | |
|---|---|---|---|---|---|---|---|
| | **1** | **2** | **3** | | **1** | **2** | **3** |
| **ABL1** | 1.00 | 52.95 | 23.97 | **CASP7** | 95.63 | -1.00 | 68.74 |
| **AKT1** | 1.00 | 1.09 | 9.44 | **CASP8** | 286.94 | 310.53 | 212.58 |
| **APAF1** | 125.12 | 131.47 | 87.91 | **CASP9** | 135.62 | 127.29 | 171.09 |
| **BAD** | 13.16 | 54.65 | -1.77 | **CD40** | 1.00 | 114.13 | -1.00 |
| **BAG1** | -22.99 | 17.13 | -21.21 | **CD40LG** | 1.00 | 52.73 | -1.00 |
| **BAG3** | -4.95 | 72.22 | -4.96 | **CFLAR** | 1.00 | 6.27 | -1.00 |
| **BAG4** | 1.00 | 49.96 | 27.51 | **CIDEA** | -1.20 | -1.20 | -1.20 |
| **BAK1** | 24.61 | 35.97 | -1.00 | **CIDEB** | 1.00 | 65.37 | -1.00 |
| **BAX** | 277.89 | 19.39 | 22.28 | **CRADD** | 89.41 | 160.41 | -1.00 |
| **BCL10** | 3.79 | 1.04 | 6.96 | **DAPK1** | 196.39 | 237.44 | -1.00 |
| **BCL2** | 11.95 | 14.53 | -1.07 | **DFFA** | 333.47 | 208.20 | 269.80 |
| **BCL2A1** | 1.00 | 1.02 | 1.52 | **FADD** | 65.34 | 87.82 | 22.53 |
| **BCL2L1** | 22.56 | -2.57 | 1.28 | **FAS** | 134.76 | 166.59 | 74.37 |
| **BCL2L10** | 1.00 | 1.81 | 1.13 | **FASLG** | 54.33 | 32.76 | 21.43 |
| **BCL2L11** | 11.27 | -2.48 | -4.54 | **GADD45A** | 28.98 | 36.98 | 22.79 |
| **BCL2L2** | -1.00 | 46.90 | -1.00 | **HRK** | 37.31 | 128.77 | 53.77 |
| **BCLAF1** | -1.00 | -1.00 | 13.29 | **IGF1R** | -19.96 | -14.16 | -3.08 |
| **BFAR** | -4.14 | 17.51 | 1.51 | **LTA** | 1.00 | 25.06 | 48.36 |
| **BID** | 33.26 | 45.21 | -8.03 | **LTBR** | 1.00 | -1.00 | 13.44 |
| **BIK** | 4.76 | 1.21 | 1.48 | **MCL1** | -2.44 | 163.63 | 1.61 |
| **NAIP** | 1.01 | 4.95 | 1.39 | **NOL3** | 528.64 | 2.75 | -1.00 |
| **BIRC2** | -2.41 | -5.14 | 1.67 | **PYCARD** | -1.00 | 11.30 | 2.33 |
| **BIRC3** | -1.41 | -5.48 | 2.89 | **RIPK2** | -1.00 | 182.77 | 232.10 |
| **XIAP** | -4.14 | -2.11 | -7.26 | **TNF** | 15.66 | 13.22 | 9.77 |
| **BIRC6** | -22.16 | 23.08 | -1.46 | **TNFRSF10A** | 1.00 | -1.00 | 2.10 |
| **BIRC8** | -14.50 | -8.94 | -3.96 | **TNFRSF10B** | 67.70 | 98.64 | -1.00 |
| **BNIP1** | 1.00 | 8.69 | 17.12 | **TNFRSF11B** | -1.00 | 780.69 | -1.00 |
| **BNIP2** | 16.48 | 8.81 | -1.00 | **TNFRSF1A** | -1.00 | -1.00 | -1.00 |
| **BNIP3** | 16.57 | -4.26 | 1.00 | **TNFRSF21** | -1.00 | 255.15 | -1.00 |
| **BNIP3L** | 37.23 | -19.08 | 29.33 | **TNFRSF25** | -1.00 | 122.29 | -1.00 |
| **BRAF** | -4.92 | -9.99 | 1.01 | **CD27** | -1.89 | 32.19 | -1.89 |
| **NOD1** | 1.21 | 70.18 | 32.43 | **TNFRSF9** | -1.00 | -1.00 | -1.00 |
| **CARD6** | -1.00 | 41.07 | 27.79 | **TNFSF10** | -1.00 | 294.96 | -1.00 |
| **CARD8** | 112.86 | 76.33 | 55.79 | **CD70** | -1.00 | 388.38 | 78.53 |
| **CASP1** | -1.00 | 399.50 | -1.00 | **TNFSF8** | -1.00 | 74.87 | 258.24 |
| **CASP10** | 63.24 | 210.64 | 98.55 | **TP53** | 2341.76 | -2.03 | 178.61 |
| **CASP14** | 1.00 | 65.32 | 26.72 | **TP53BP2** | 224.61 | -12.31 | -13.85 |
| **CASP2** | 23.51 | 43.34 | -1.00 | **TP73** | 1.00 | 2399.65 | 3188.38 |
| **CASP3** | 187.64 | 2.03 | 53.19 | **TRADD** | 101.66 | 743.72 | 342.89 |
| **CASP4** | 17.80 | 52.30 | -9.79 | **TRAF2** | 1.00 | 2103.55 | -1.00 |
| **CASP5** | 1.00 | 140.07 | -1.00 | **TRAF3** | -1.00 | 665.37 | 322.04 |
| **CASP6** | 80.39 | 27.91 | -1.00 | **TRAF4** | -1.00 | 472.43 | -1.00 |

a Data represent mean of samples **1**-**3**-induced fold-change in gene expression relative to control-treated cells (n = 3), $p < 0.05$. Up-regulated genes; Down-regulated genes.

release. In short, mitochondrial membrane permeability is regulated through a family of proto-oncogenes. Anti-apoptotic (BCL-2) or pro-apoptotic (BAD, BAX) proteins comprise the BCL-2 family of proto-oncogenes [53]. Once activated, BAX is inserted into the mitochondrial membrane, increasing membrane permeability leading to apoptosis [54]. Anti-apoptotic BCL-2 inhibits the ability of BAX to increase membrane potential [55]. In the treated MCF-7R cells, BCL-2 was down-regulated (Table 3), allowing for apoptosis.

As p73 is localised in the nucleus and during the induction of cell death remains localised there, any influence of p73 on Bax translocation is indirect. Therefore, the p73 isoform, TAp73, exerts two distinct effects on Bax: (i) direct transactivation of the promoter to enhance the steady state protein levels of Bax, and (ii) indirect mitochondrial translocation of Bax protein from the cytosol to the mitochondrial membranes [56]. The loss of mitochondrial transmembrane potential is likely to be the initial event leading to apoptosis [57] with concomitant reduction of the mitochondrial inner membrane potential, $\Delta\Psi m$, disturbance of the outer mitochondrial membrane and consequent loss from the intermembrane region of proteins such as cytochrome c [58].

Cytochrome c, which binds to apoptotic activating factor-1 (APAF-1), was also significantly expressed in MCF-7R cells treated with **1**–**3** (Table 3) and is known to activate caspase-9 (Fig. 9; Tables 3 and 4) leading in turn to the activation of caspase-3 (Fig. 10; Tables 3 and 5); caspase-3 is the most potent effector caspase with many substrates. It is thought that mitochondrial-induced apoptosis may also involve a caspase-independent pathway. Compound **2**, which triggers low expression of caspase-3 (2.03-fold) in the PCR array analysis, exhibited the lowest cytotoxicity on MCF-7R cells of the gold compounds evaluated. Referring to Fig. 8, after an apoptotic stimulus, an increase in mitochondrial membrane potential allows for the release of apoptosis-inducing factor (AIF), which activates a DNase leading to apoptosis [59,60].

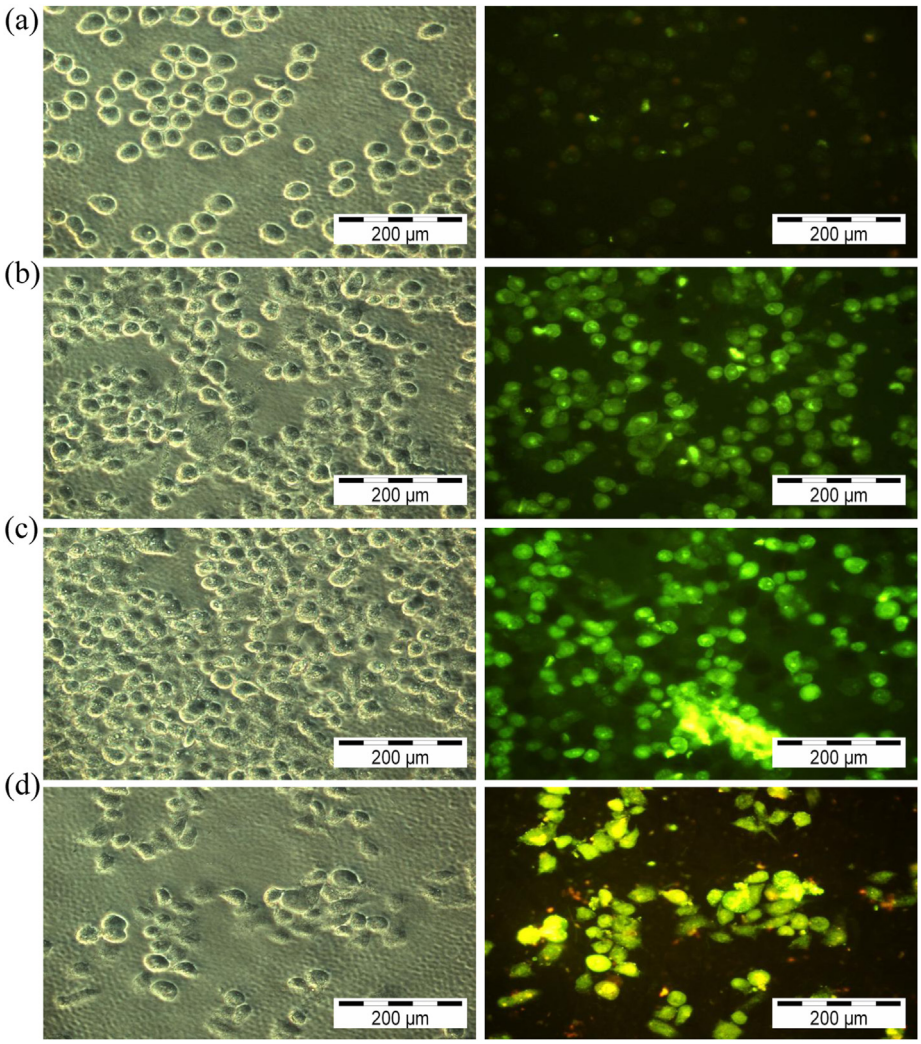


**Fig. 9.** In situ caspase-9 detection. The MCF-7R cells were cultured for 24 h in control media, (a), and in the presence of 4.4 μM **1** (b), 13.6 μM **2** (c), and 9.3 μM **3**, (d) caspase-9 (green) was detected using the fluorescent caspase-9 substrate (FAM-LEHD-FMK). Notes: (a) little detection of caspase-9 is seen in control MCF-7R cells using the substrate detection assay. (b), (c) and (d) show robust caspase-9 detection is seen in MCF-7R cells cultured in the presence of **1**, **2** and **3**, respectively. (For interpretation of the references to colour in this figure legend, the reader is referred to the web version of this article.)

In the extrinsic pathway, the death pathways involving death receptors such as Fas and TNFR1, of the tumour necrosis factor (TNF) family, are well understood in that they recruit FADD and procaspase-8 and procaspase-10 to the receptor. Recruitment mediated by FADD of procaspase-8 and procaspase-10 leads to its auto-cleavage and activation, and in turn causes cell death by activating effector caspases such as caspase-3 [61,62]. Among the death pathways, the Fas/FasL system is a key signal pathway involved in apoptosis regulation in several different cell types [63,64]. The present study showed that treatment of MCF-7R cells with **1**–**3** increased FAS gene expression. In turn, caspase-8, caspase-9, caspase-10 and caspase-3 were activated with an increase in their enzymatic activities (Figs. 9–11; Tables 3–5).

It is possible that caspase-8 and caspase-10 could also cleave the BCL-2 family member Bid, a BH3 interacting domain death agonist, to truncated BID (tBID), which binds to the pro-apoptotic protein BAX, resulting in $\Delta\Psi m$ disruption and the release of cytochrome c [65,66]. BID is generally considered as a molecular linker bridging death receptor and mitochondria pathways [67]. Compounds **1**–**3** also induced up-regulation of BID expression in MCF-7R cells (Table 3), which provides additional supporting evidence for the proposed apoptotic pathways.

**Table 4**
Quantification of caspase 3, 7, 8, 9-positive MCF-7R cells in RPMI 1640 cultured in the presence of **1**, **2** and **3**.[a]

| Caspase | Control | Absorbance | | |
|---|---|---|---|---|
| | | **1** | **2** | **3** |
| Caspase-3/7 | 79 ± 0.3 | 11,811 ± 0.3 | 977 ± 0.2 | 8795 ± 0.3 |
| Caspase-8 | 83 ± 0.2 | 45,737 ± 0.3 | 10,671 ± 0.3 | 16,161 ± 0.3 |
| Caspase-9 | 88 ± 0.2 | 28,433 ± 0.3 | 10,905 ± 0.2 | 15,820 ± 0.2 |

[a] The green fluorescent signal (Figs. 9–11) is a direct measure of the amount of active caspases present in the cells at the time the reagent was added. Excitation wavelength = 490 nm and emission wavelength = 520 nm. The reported values represent the mean and standard deviation of at least two independent experiments run, each run in triplicate.

### 2.7. Measurement of reactive oxygen species (ROS) production

It was thought of interest to also determine whether the observed cytotoxicity of **1**–**3** was correlated with the generation of reactive oxygen species (ROS). Hence, the production of cellular

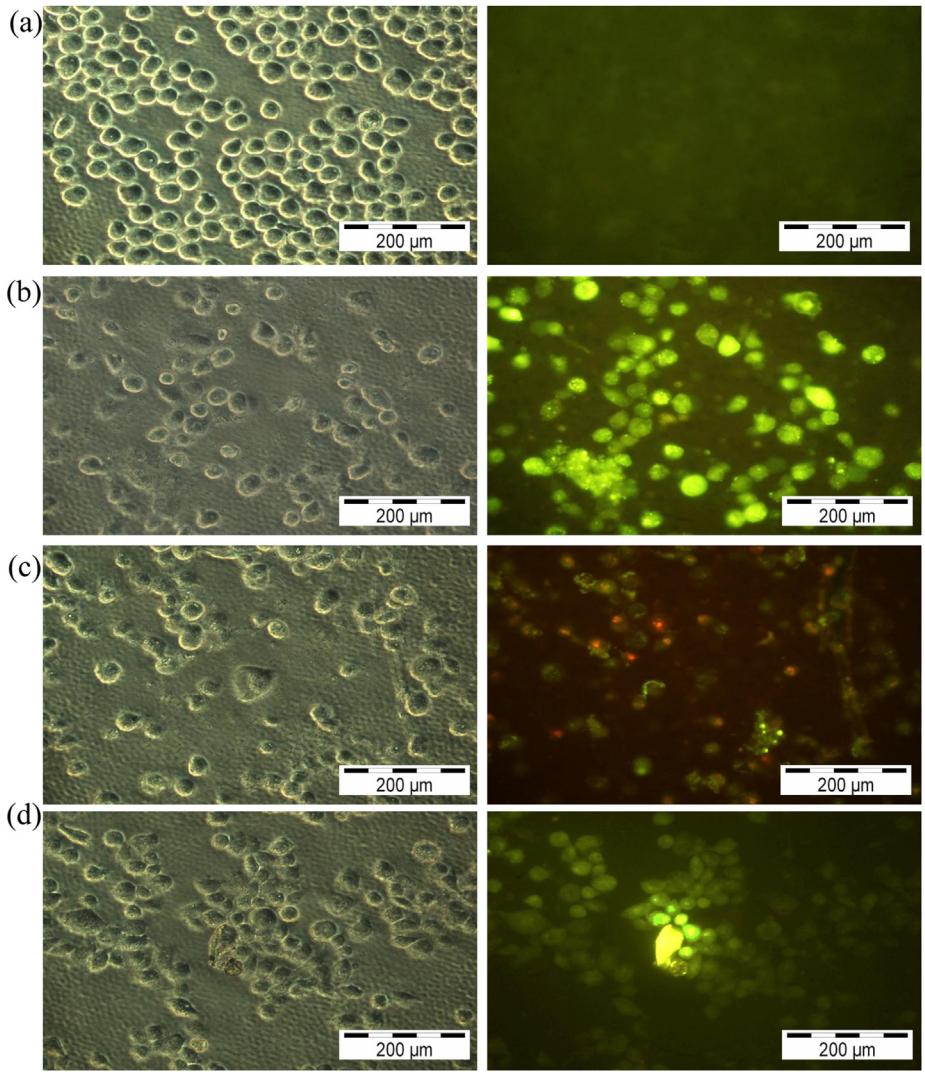


**Fig. 10.** In situ caspase-3/7 detection. The MCF-7R cells were cultured for 24 h in control media, (a), and in the presence of 4.4 μM **2** (b), 13.6 μM **3** (c) and 9.3 μM **4**, (d) caspase-3/7 (green) was detected using the fluorescent caspase-3,7 substrate (FAM-DEVD-FMK). Notes: (a) no detection of caspase-3/7 is seen in control MCF-7R cells using the substrate detection assay. (b), (c) and (d) show robust caspase-3/7 detection is seen in MCF-7R cells cultured in the presence of **1**, **2** and **3**. (For interpretation of the references to colour in this figure legend, the reader is referred to the web version of this article.)

ROS (mainly $H_2O_2$) was analysed using the fluorogenic freely permeable tracer, DCFH-DA. Intracellular esterases deacylate DCFH-DA to DCFH, a non-fluorescent compound, and through the action of peroxides in the presence of ROS, oxidises DCFH-DA to the fluorescent compound, DCF [68,69]. In the presence of **1**–**3**, cellular ROS generation exceeded 5-fold that of the negative control (untreated cells), indicating that the trial compounds induce significant $H_2O_2$ generation (Fig. 12). Many reports have shown that ROS generation may be either a cause or a consequence of the PTP opening and mitochondrial alterations in apoptosis [70,71]. The mitochondria are a source of ROS and, simultaneously, a target of excessive ROS generation. Excess ROS increases the mitochondrial membrane permeability and damages the respiratory chain resulting in further ROS production [72]. The disruption in the mitochondrial membrane causes the release of cytochrome c from the mitochondria, which initiates events leading to apoptosis. Although the exact mechanism is undefined, ROS are thought to play a role in TNFR and FAS receptor-mediated apoptosis [73].

One of the topics attracting considerable attention in research of apoptosis is the switch mechanism of the cell death mode from apoptosis to necrosis: a body of experimental data is accumulating which demonstrates that some chemicals cause apoptotic changes followed by necrosis [74,75]. Whereas apoptotic cells undergo phagocytization by neighbouring cells, necrotic cells cause general and localised reactions. During normal development, embryogenesis and morphogenesis rely on the key role played by apoptosis but this can also be induced, with detrimental effects, by oxidative stress and other pathological conditions. Cell death

**Table 5**
Quantification of AFC in MCF-7R cells cultured in the presence of sample **1**, **2** and **3** upon cleavage of the AEVD-AFC substrate by caspase-10.[a]

| Caspase | Control | Absorbance | | |
|---|---|---|---|---|
| | | **1** | **2** | **3** |
| Caspase 10 | 86 ± 0.3 | 13,399 ± 0.3 | 16,851 ± 0.3 | 19,439 ± 0.2 |

[a] AEVD-AFC emits blue light ($\lambda_{max}$ = 400 nm). Upon cleavage of the substrate by caspase-10, free AFC emits a yellow-green fluorescence ($\lambda_{max}$ = 505 nm). The reported values represent the mean and standard deviation of at least two independent experiments run, each run in triplicate.

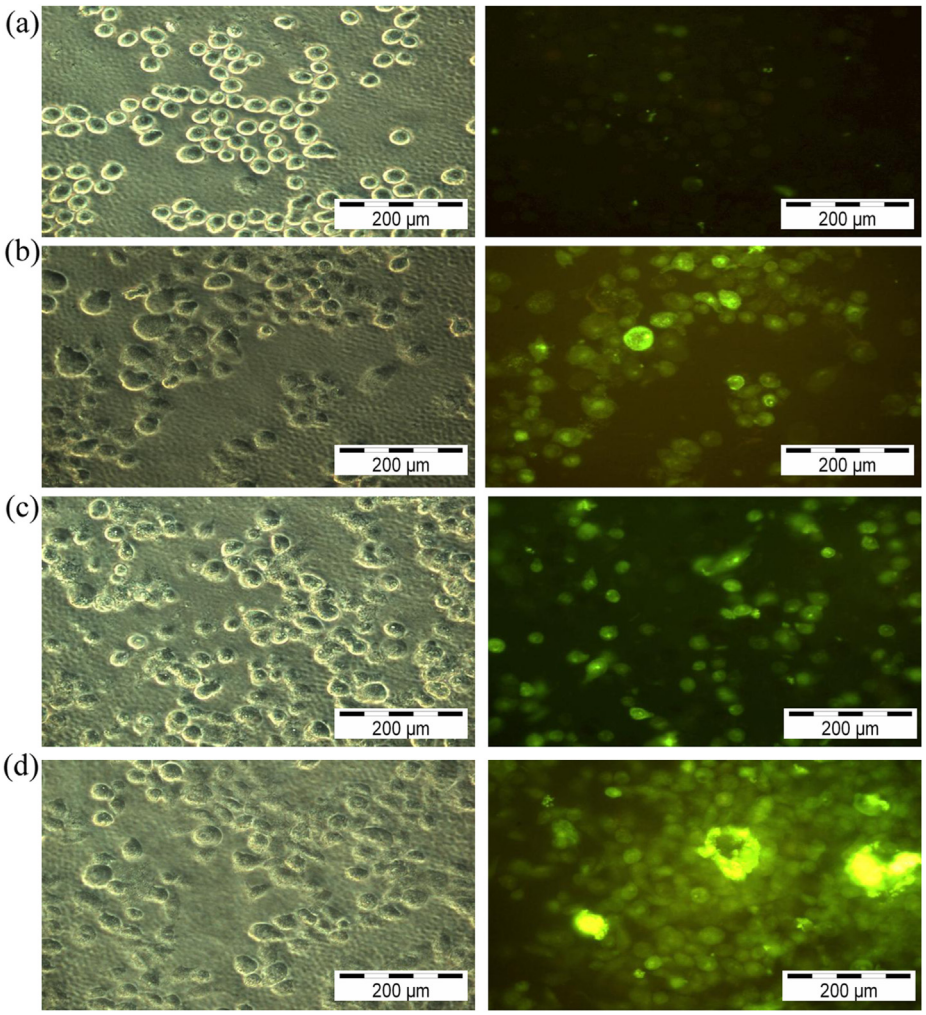


**Fig. 11.** In situ caspase-8 detection. The MCF-7R cells were cultured for 24 h in control media, (a), and in the presence of 4.4 μM **1** (b), 13.6 μM **2** (c) and 9.3 μM **3**, (d) caspase-8 (green) was detected using the fluorescent caspase-8 substrate (FAM-LETD-FMK). (a), little detection of caspase-8 is seen in control MCF-7R cells using the substrate detection assay. (b), (c) and (d), Robust caspase-8 detection is seen in MCF-7R cells cultured in the presence of **1**, **2**, **3**. (For interpretation of the references to colour in this figure legend, the reader is referred to the web version of this article.)

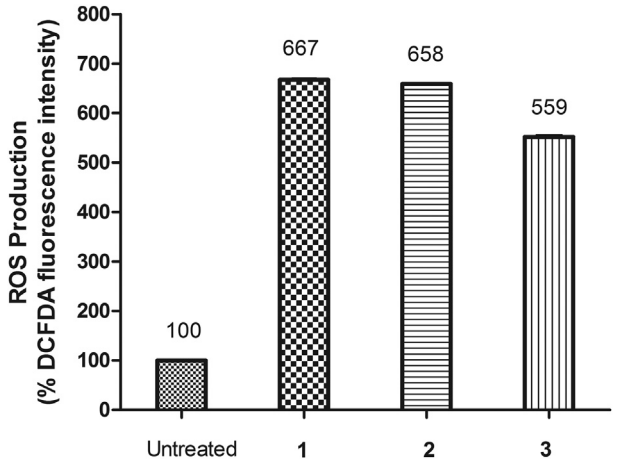


**Fig. 12.** Production of ROS after treatment of MCF-7R cells with **1**–**3**, at doses corresponding to their $IC_{50}$ values (4.4, 13.6 and 9.3 μM, respectively) for 16 h. After labelling with carboxy-H2DCFDA for 1 h, the fluorescence was measured.

by necrosis arises from an acute disruption of cellular metabolism, leading to the depletion of ATP, ion dysregulation, swelling of cells and mitochondria, the activation of degradative enzymes, failure of plasma membrane as well as cell lysis [76]. Acute cytotoxicity causing necrotic cell death differs from apoptosis or programmed cell death [77]. Generally, apoptosis can develop when ATP is high, but when ATP is low necrotic cell death occurs instead. The onset of the mitochondrial permeability transition causes mitochondrial uncoupling, ATP depletion and necrotic cell death provided the cell is solely dependent on oxidative phosphorylation for ATP. In circumstances where glycolysis elevates levels of ATP, it is possible that ATP production persists despite the mitochondrial permeability transition, to allow cells to undergo apoptosis [78–80]. Another proposal is that the switch mechanism of cell death mode from apoptosis to necrosis occurs as a result of burst in the intracellular level of ROS [81,82]. As seen in Fig. 6, the majority of MCF-7R cells underwent necrosis process after treatment with **2** and **3**, along with high ROS production (Fig. 12). The present study suggests that a burst in the intracellular level of superoxide may be intimately related to the switch of the cell death mode from apoptosis to necrosis. Interestingly, while **1** exhibits the oxidative burst, no evidence was found for necrosis.

As seen from Table 3, DAPk1, death-associated protein kinase 1, was highly expressed upon treatment with **1** and **2** (about 196- and 237-fold, respectively). DAPk1 is a member of a newly classified family of Ser/Thr kinases which is regulated by calcium/calmodulin, and is known as a tumour suppressor, important to effectors determining cellular functions such as cell motility, survival, autophagy and death [83–86]. The DAPk family has been linked to the activity of various cell death integrated signalling pathways and molecular functions other than apoptosis. DAPk1 inhibited the protein expression of anti-proliferation genes such as COX-2, anti-invasion related protein, ICAM-1, and anti-apoptosis genes such as X-linked mammalian inhibitor of apoptosis protein (XIAP). Moreover, over-expression of DAPk1 significantly rescued the protein expression levels of NF-κB-targeted genes. DAPk1 has been confirmed in regulating NF-κB activation through TNF-α or INF-γ-stimulated apoptosis in OVCAR-3 carcinoma cells [87]. NF-κB plays a critical role in regulating the expression of target genes, including cell survival, apoptosis, invasion and inflammatory processes. Activated NF-κB translocates to the nucleus and activates transcription of target genes such as inhibitors of apoptosis proteins (IAP's), XIAP and survivin protein through its binding ability to specific sequences of caspase-3 or -9 DNA. In addition, many cancer cells and tumour specimens have high levels of XIAP, and its inactivation results the apoptosis [88]. Interestingly, XIAP was down-regulated with compound **1**–**3** (Table 3).

Finally, DFFA, DNA fragmentation factor subunit alpha, was significantly expressed after treatment of **1**–**3** (Table 3). DFFA is an inhibitor of caspase-activated DNase (ICAD), a protein that in humans is encoded by the DFFA gene, is the substrate for caspase-3 and during apoptosis triggers DNA fragmentation. When DFFA is cleaved by caspase-3, DFF becomes activated; the cleaved fragments of DFFA dissociate from DFFB, the active component of DFF. DFFB has been found to trigger both DNA fragmentation and chromatin condensation during apoptosis [89].

### 2.8. Human topoisomerase I inhibition study

Topoisomerases are key enzymes that control the topological state of DNA by means of the breaking and rejoining of DNA strands. There are two classes of topoisomerases: (i) the type I enzymes which act by transiently nicking one of the two DNA strands, and (ii) type II enzymes which nick both DNA strands and whose activity is dependent on the presence of ATP. A significant number of vital cellular processes that influence DNA replication require the participation of these enzymes [90,91], e.g., transcription, recombination, integration and chromosomal segregation. Accordingly, some anti-tumour agents target topoisomerases and act through different mechanisms dependent on the different catalytic steps, which either inhibit the enzyme catalytic cycle or stabilise the cleavage complex in which the DNA is cleaved and covalently linked to the enzyme [92–94]. Topoisomerase I (topo I) inhibitors are among the most widely used anti-cancer drugs as they possess a variety of anti-tumour properties [95–97]. Accordingly, it was thought worthwhile to evaluate the potential of **1**–**3** and dithiocarbamate anion (**4**) to inhibit topo I.

In the DNA relaxation assay employed herein, one unit of human topo I can completely convert all the supercoiled plasmid pBR322 (4.4 kb) to the fully relaxed topoisomer, which is the completely unwound covalently bonded closed circular DNA (Fig. 13(a)–(d), lane 4). This, labelled Form II in Fig. 13, is the slowest moving DNA band and contains the fully relaxed closed circular pBR322 and a small amount of the originally present nicked DNA [94]; the difference in plasmid size may account for the inability to separate the fully relaxed pBR322 from the nicked pBR322. Incubating pBR322 with the highest concentrations of **1**–**4** (0.125–6.0 μM) resulted in

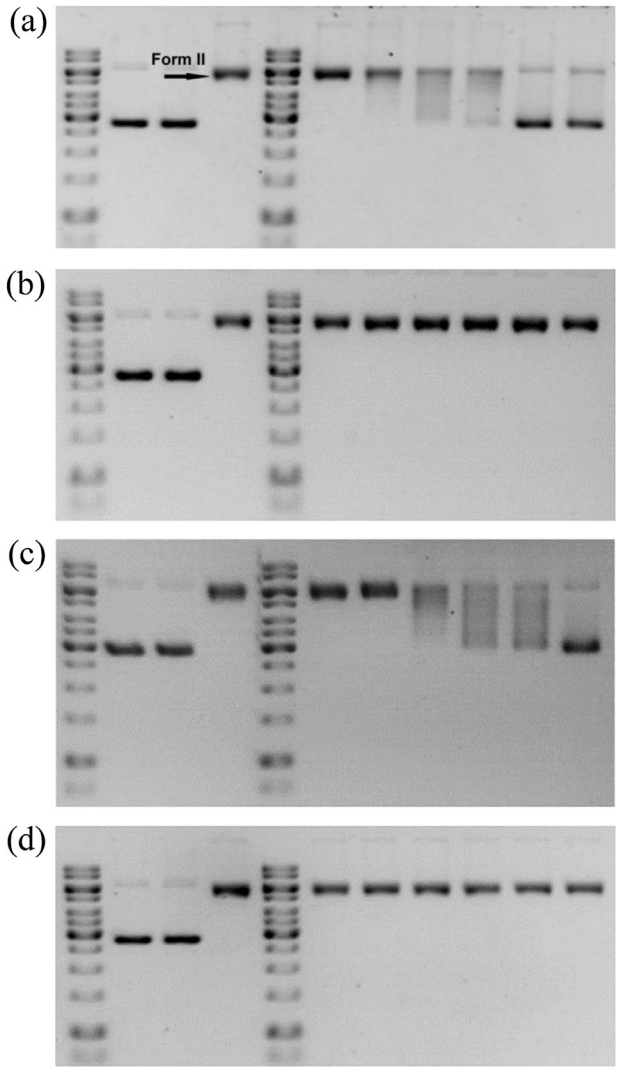


**Fig. 13.** Human topoisomerase I inhibition assay by gel electrophoresis. Electrophoresis results of incubating human topoisomerase I (1 unit/21 μL) with pBR322 (0.25 μg) in the absence or presence of 0.125–6.0 μM of (a) **1**, (b) **2**, (c) **3** and (d) **4**: lanes 1 & 5, gene ruler 1 kb DNA ladder; lane 2, DNA alone; lane 3, DNA + 4.0 μM compound (control); lane 4, DNA + 1 unit human topoisomerase I (control); lane 6, DNA + 0.125 μM compound + 1 unit human topoisomerase I; lane 7, DNA + 0.5 μM compound + 1 unit human topoisomerase I; lane 8, DNA + 1.0 μM compound + 1 unit human topoisomerase I; lane 9, DNA + 2.0 μM compound + 1 unit human topoisomerase I; lane 10, DNA + 4.0 μM compound + 1 unit human topoisomerase I; lane 11, DNA + 6.0 μM compound + 1 unit human topoisomerase I.

no cleavage or unwinding of the DNA as the banding pattern is the same as the control (Fig. 13(a)–(d), lane 3). However, when pBR322 was incubated with human topo I and increasing concentrations of **1** and **3**, a reduction of the nicked band (containing nicked and fully relaxed DNA) was observed as was the formation of various faster moving bands of topoisomers with different degrees of relaxation (Fig. 13(a) and (c), lanes 7–9). At 1.0 μM of **2** and **4**, an unchanged supercoiled DNA band starts to appear (Fig. 13(b) and (d), lane 8). The appearance of slower moving bands of less relaxed topoisomers was observed with increasing concentrations of **1** and **3** (Fig. 13(a) and (c), lanes 6–11). These results showed that **1** and **3** are able to inhibit the function of topo I by relaxing the supercoiled pBR322, and also show that the degree of inhibition is dependent on concentration. The above also indicates that **1** and **3** are topo I inhibitors and not topo I poisons, which prevents the nicked DNA from relegation. Compounds **1** and **3** exhibit a full inhibitory

activity on topo I at concentrations of 4.0 and 6.0 μM, respectively. Compound **1** started to show topoisomers at 0.5 μM. By contrast, **3** showed the lowest inhibitory capability on topo I at 50% higher the concentration of compound **1** in achieving full inhibition on topo I activity (Fig. 13(a) and (c), lanes 6–11).

Interestingly, no inhibitory activity of topo I was observed in the presence of **2** and **4** as the DNA bands are the same as those observed for DNA incubated only with topo I (Fig. 13(b) and (d), lanes 6–11). Further investigations in mechanisms of topo I inhibition by **1** and **3** are underway.

## 3. Conclusions

The $R_3PAu[S_2CN(^iPr)CH_2CH_2OH]$, for R = Ph (**1**), Cy (**2**) and Et (**3**), compounds are cytotoxic against the doxorubicin-resistant breast cancer cell line, MCF-7R, with **1** being the most potent and more cytotoxic than either of doxorubicin and cisplatin. The mechanism of cell death caused by **1** is apoptotic, while cell death induced by **2** and **3** is necrotic; both extrinsic and intrinsic pathways are evident. Compound **1** activates the p53 gene, **2** activates only the p73 gene, whereas **3** activates both the p53 and p73 genes. Compounds **1** and **3** are shown to activate NF-κB. Compounds **1** and **3** inhibit topoisomerase I.

In a recent study of related $Ph_3PAu[SC(OR)=NPh]$, R = Me, Et, $^i$Pr, compounds, where comparable experimental protocols were employed, but against the HT-29 colon cancer cell line [98], equally dramatic changes in mechanism of cell death were noted, this time as R in the thiolate ligand was varied. From the foregoing, it is clear further work is required to evaluate the potential of these compounds as anti-cancer agents, their mechanisms of action and even to ascertain the chemically desirable features, that is phosphane- and thiolate-bound R groups, of the compounds themselves.

## 4. Experimental

### 4.1. Instrumentation

$^1$H and $^{13}C\{^1H\}$ NMR spectra were recorded in $CDCl_3$ solution at 25 °C on JOEL LA and JOEL Lambda 400 MHz NMR spectrometers with chemical shifts referenced to the residual proton of $CDCl_3$. $^{31}P\{^1H\}$ NMR spectra were recorded in $CDCl_3$ solution at 25 °C on a Bruker Avance 400 MHz NMR spectrometer with the chemical shifts recorded relative to 85% aqueous $H_3PO_4$ as external reference; abbreviations for NMR assignments: *s*, singlet; *d*, doublet; *t*, triplet; *q*, quartet; *sept*, septet; *m*, multiplet. Scheme 2 shows the numbering scheme adopted for the NMR spectra; spectra for **1**–**3** are given in Tables S(5)–S(7), respectively. IR spectra were obtained by an Attenuated Total Reflectance (ATR) technique on a Perkin Elmer RX1 FTIR spectrophotometer; abbreviations: *s* = strong, *m* = medium, *w* = weak, *sh* = sharp and *br* = broad. Elemental analyses were performed on a Perkin Elmer PE 2400 CHN Elemental Analyser. Melting points were determined on a Mel-Temp II melting point apparatus.

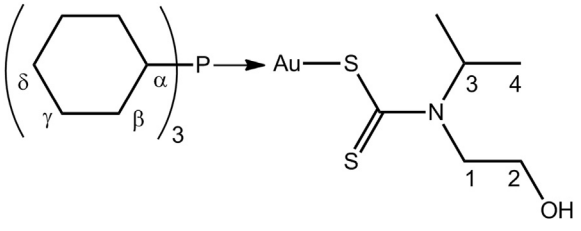


**Scheme 2.** Numbering scheme employed the NMR spectroscopic study.

### 4.2. Synthesis

All reactions were carried out under ambient conditions. All chemicals and solvents were used as received and without further purification. The $R_3PAuCl$ precursors were synthesised by reducing $HAuCl_4$ with sodium sulfite followed by addition of the respective $R_3P$, while $Na[S_2CN(^iPr)CH_2CH_2OH]$ was prepared in quantitative yield from the reaction of $HN(^iPr)CH_2CH_2OH$ with NaOH and $CS_2$. Analyses (C, H, N) were within ±0.4% of the theoretical values.

#### 4.2.1. Synthesis of $Ph_3PAu[S_2CN(^iPr)CH_2CH_2OH]$ (**1**)

$Na[S_2CN(^iPr)CH_2CH_2OH]$ (0.20 g, 1 mmol) in water (20 ml) was added drop wise to a suspension of $Ph_3PAuCl$ (0.49 g, 1 mmol) in acetone (10 ml) and was stirred for 1 h to give a yellow gum. This was stirred in $Et_2O$ for 1 h and the solvent was decanted, leaving the gum to dry at room temperature which yielded a yellow powder in 60% yield; M.P. 136 °C. Anal. Calc.: C, 45.22; H, 4.27; N, 2.20. Found: C, 44.97; H, 3.91; N, 2.08%. IR ($cm^{-1}$): 3361*br*, *w* ν(O–H); 2972*w* ν(C–H); 1586*w* ν(C=C); 1434*s*, *sh* ν(C–N); 1027 $\nu(CS_2)_{asym}$; 997*m*, *sh* $\nu(CS_2)_{sym}$. $^1$H NMR ($CDCl_3$): δ 1.25 (*d*, 6H, H4, $^3J_{H-H}$ = 6.8 Hz), 3.18 (*s*, 1H, OH), 3.92 (*t*, 2H, H1, $^3J_{H-H}$ = 4.0 Hz), 4.01 (*t*, 2H, H2, $^3J_{H-H}$ = 5.6 Hz), 5.39 (*sept*, 1H, H3, $^3J_{H-H}$ = 6.8 Hz), 7.46–7.57 (*m*, 15H, Hα-δ) ppm. $^{13}C\{^1H\}$ NMR ($CDCl_3$): δ 20.4 (C4), 29.8 (C1), 56.4 (C2), 63.0 (C3), 129.2 (Cγ), 129.3 (Cα), 132.0 (Cδ), 134.3 (Cβ), 208.7 ($C_{quat}$) ppm. $^{31}P\{^1H\}$ NMR ($CDCl_3$): δ 33.6 ppm.

#### 4.2.2. Synthesis of $Cy_3PAu[S_2CN(^iPr)CH_2CH_2OH]$ (**2**)

$Na[S_2CN(^iPr)CH_2CH_2OH]$ (0.20 g, 1 mmol) in water (20 ml) was added drop wise to a suspension of $Cy_3PAuCl$ (0.51 g, 1 mmol) in acetone (10 ml). The mixture was stirred for 1 h giving a yellow solid, which was filtered, washed with water and allowed to dry at room temperature to yield 53% of **3**; M.P. 146 °C. Anal. Calc.: C, 43.97; H, 6.92; N, 2.14. Found: C, 43.85; H, 7.18; N, 2.07%. IR ($cm^{-1}$): 3437*br*, *w* ν(O–H); 2925*s*, *sh* ν(C–H); 1440*s*, *sh* ν(C–N); 1051*s*, *sh*, $\nu(CS_2)_{asym}$; 965*m*, *sh* $\nu(CS_2)_{sym}$. $^1$H NMR ($CDCl_3$): δ 1.22–1.31 (*m*, H4), 1.50–1.54 (*m*, Hδ), 1.65–1.75 (*m*, Hγ), 1.84–1.86 (*m*, Hβ), 2.00–2.03 (*m*, Hα), 3.37 (*t*, OH, $^3J_{H-H}$ = 6.0 Hz), 3.92 (*q*, 2H, H1, $^3J_{H-H}$ = 5.3 Hz), 4.02 (*t*, 2H, H2, $^3J_{H-H}$ = 6.0 Hz), 5.40 (*sept*, 1H, H3, $^3J_{H-H}$ = 6.0 Hz) ppm. $^{13}C\{^1H\}$ NMR ($CDCl_3$): δ 20.2 (C4), 25.9 (Cδ), 27.1 (Cγ), 30.5 (Cβ), 33.5 (Cα), 49.6 (C1), 55.7 (C2), 63.0 (C3), 208.9 ($C_{quat}$) ppm. $^{31}P\{^1H\}$ NMR ($CDCl_3$): δ 54.0 ppm.

#### 4.2.3. Synthesis of $Et_3PAu[S_2CN(^iPr)CH_2CH_2OH]$ (**3**)

$Na[S_2CN(^iPr)CH_2CH_2OH]$ (0.20 g, 1 mmol) in a minimum amount of water (20 ml) was added drop wise to a suspension of $Et_3PAuCl$ (0.35 g, 1 mmol) in acetone (10 ml). The mixture was stirred for 1 h after which a bright-yellow solid precipitated. This was filtered off, washed with water and allowed to dry at room temperature to yield 63% of **3**; M.P. 80 °C. Anal. Calc.: C, 29.22; H, 5.52; N, 2.84. Found: C, 29.3; H, 5.93; N, 2.70%. IR ($cm^{-1}$): 3360*br*, *m* ν(O–H); 2964*w*, *sh* ν(C–H); 1452*s*, *sh* ν(C–N), 1038*s*, *sh* $\nu(CS_2)_{asym}$, 968*m*, *sh* $\nu(CS_2)_{sym}$. $^1$H NMR ($CDCl_3$): δ 1.19–1.28 (*m*, 15H, $H_1$, $H_\beta$), 1.80–1.88 (*m*, 6H, $H_\alpha$), 3.26 (*s*, 1H, OH), 3.92 (*t*, 2H, H1, $^3J_{H-H}$ = 5.6 Hz), 4.01 (*t*, 2H, H2, $^3J_{H-H}$ = 5.6 Hz), 5.39 (*sept*, 1H, H3, $^3J_{H-H}$ = 5.6 Hz) ppm. $^{13}C\{^1H\}$ NMR ($CDCl_3$): δ 9.0 (Cβ), 18.7 (Cα), 20.3 (C4), 49.7 (C1), 56.0 (C2), 62.9 (C3), 208.5 ($C_{quat}$) ppm. $^{31}P\{^1H\}$ NMR ($CDCl_3$): δ 34.1 ppm.

### 4.3. X-ray crystallography

Crystals of **2** and **3** suitable for X-ray diffraction were obtained by slow evaporation of tetrahydrofuran and chloroform, respectively. X-ray diffraction measurements for **2** and **3** were performed at 100 K on an Agilent Supernova dual diffractometer with an Atlas (Mo) detector employing the ω scan technique and using graphite monochromatized Mo Kα radiation so that $\theta_{max}$ was 27.6° [99].

Crystal data are given in Table 6. The structures were solved by direct methods (SHELXS97 [100] through the WinGX Interface [101]) and refined (anisotropic displacement parameters, H atoms in the riding model approximation and a weighting scheme of the form $w = 1/[\sigma^2(F_o^2) + aP^2]$ where $P = (F_o^2 + 2F_c^2)/3$) with SHELXL97 on $F^2$ [×2]. In each refinement, some reflections {**2**: (0 1 17), (1 0 1) and (−1 1 17); **3**: (−3 −1 9) and (−7 −3 2)} were omitted owing to poor agreement. In **3**, the absolute structure was determined on the basis of Friedel pairs included in the data set. Finally, for **3**, the maximum and minimum residual electron density peaks of 1.50 and 0.76 e Å$^{-3}$, respectively, were located 0.90 and 0.64 Å from the Au1 atom, respectively. The molecular structures shown in Figs. 1 and 2, were drawn with 50% displacement ellipsoids [101]. The overlay diagram, Fig. 3, was drawn with QMol [102] and the crystal packing diagrams with DIAMOND [103].

### 4.4. Cell culture and inhibition of cell growth

The human MCF-7R breast cancer cell line was obtained from ATCC: The Global Bioresource Center and maintained in culture as described by the provider. The cells were routinely grown in RPMI 1640 medium containing 10% foetal calf serum (FCS) and antibiotics at 37 °C and 6% $CO_2$. For evaluation of growth inhibition tests, the cells were seeded in 96-well plates (Techno Plastic Products, TPP, Plastik für die Zellkultur, Switzerland) and grown for 24 h in complete medium. The stock solutions of the trial compounds were prepared by dissolving the compounds in 1 ml of DMSO to reach a concentration of $10^{-2}$ M. They were then diluted in RPMI medium and added to the wells (100 μL) to obtain a final concentration ranging between 0 and 80 μM. DMSO at comparable concentrations did not show any effects on cell cytotoxicity. Stock solutions of the compounds were diluted directly in culture medium to the required concentration and added to the cell culture. After 24 h incubation at 37 °C, 20 μL of a solution of MTT (3-[4,5-dimethylthiazole-2-yl]-2,5-diphenyltetrazolium bromide) in PBS (2 mg mL$^{-1}$) was added to each well, and the plates were then incubated for 2 h at 37 °C. The medium was then aspirated and DMSO (100 μL) was added to dissolve the precipitate. The absorbance of each well was measured at 580 nm using a 96-well microplate reader and compared to the values of control cells incubated without test compound. The $IC_{50}$ values for the inhibition of cell growth were determined by fitting the plot of the percentage of surviving cells against the drug concentration using a sigmoidal function (Origin v7.5).

**Table 6**
Crystallographic and refinement details for **2** and **3**.

| Compound | **2** | **3** |
|---|---|---|
| Formula | $C_{24}H_{45}AuNOPS_2$ | $C_{12}H_{27}AuNOPS_2$ |
| Formula weight | 655.67 | 493.40 |
| Crystal colour/habit | Yellow prism | Colourless prism |
| Crystal dimensions/mm | 0.04 × 0.06 × 0.12 | 0.05 × 0.05 × 0.10 |
| Crystal system | Monoclinic | Monoclinic |
| Space group | $P2_1/n$ | $P2_1$ |
| $a$/Å | 10.4647(3) | 11.5458(12) |
| $b$/Å | 10.8268(3) | 8.9567(10) |
| $c$/Å | 23.5694(6) | 17.386(9) |
| $\beta$/° | 97.936(2) | 107.35(3) |
| $V$/Å$^3$ | 2644.82(13) | 1716.1(9) |
| $Z$ | 4 | 4 |
| $D_c$/g cm$^{-3}$ | 1.647 | 1.910 |
| $F$(000) | 1320 | 960 |
| $\mu$(Mo $K\alpha$)/mm$^{-1}$ | 5.797 | 8.899 |
| Measured data | 10,670 | 12,889 |
| $\theta$ range/° | 2.6–27.6 | 2.5–27.6 |
| Unique data | 6065 | 7812 |
| Observed data ($I \geq 2.0\sigma(I)$) | 5192 | 7365 |
| $R$, obs. data; all data | 0.026; 0.054 | 0.034; 0.072 |
| $a$ in weighting scheme | 0.012 | 0.028 |
| $R_w$, obs. data; all data | 0.037; 0.047 | 0.039; 0.075 |
| Residual electron density peaks/e Å$^3$ | 0.74, −0.98 | 1.50, −0.76 |

### 4.5. Extraction of RNA, and RT$^2$ Profiler PCR microarray

Total RNA was extracted from cultured MCF-7R cells using a high-purity RNA Isolation Kit (Qiagen, Germany). The real-time PCR for microarray assay was performed using the RT$^2$ Profiler PCR microarray according to the manufacturer's protocol (Qiagen, USA). Gene expression was compared according to the CT value. Results are based on.

### 4.6. Caspase activity (Caspases-3, -7, -8, -9 and -10)

Caspase activity was assayed by measuring the light intensity using a kit (Caspase Assay, Milipore) and a luminometer (Perkin Elmer HTS 7000, France). Briefly, cells were cultured in 96-well plates in a final volume of 200 ml. Then 50 ml caspase reaction buffer was added and incubated at room temperature for 1 h before measurement.

### 4.7. Membrane permeability study by AOPI staining

MCF-7R cells at a concentration of 5 × 10$^3$ cells/well in 96-well plates were treated with the $IC_{50}$ concentration of each compound and incubated for 24 h. Untreated cells were included as a negative control. Treated cells were harvested from the culture flask. 1× EDTA free-PBS was used to wash the cells twice before transferring to a microcentrifuge tube. The cells were centrifuged at 1000 g for 10 min. Subsequently, the cells were suspended in 100 μL 1× PBS. Then, a 5 mg/mL acridine orange (AO) (Sigma) and propidium iodide (PI) (Sigma) mixture was added to the cells at 1:1 ratio for staining. This was followed by chilling on ice for 10 min. The mixture (20 μL) was aliquoted onto a slide and covered with a cover slip and viewed under an Olympus BX-51 fluorescence microscope. Images were captured by an attached Olympus CMAD-2 camera. The mode of cell death was then determined.

### 4.8. Intracellular reactive oxygen species (ROS) measurements

5-(and-6)-Carboxy-2′,7′-dichlorodihydrofluorescein diacetate (carboxy-H2DCFDA) (Sigma, USA) was used to detect intracellular ROS according to the manufacturer's instructions. For ROS quantification, cells were seeded in 96-well black plates (Greiner Bio-One, France) and treated with the trial compound at the indicated $IC_{50}$ concentrations for 24 h. Afterwards, cells were washed with PBS and incubated with 10 μM carboxy-H2DCFDA in DPBS for an hour. Cells were then washed and fluorescence was measured by a plate reader (Perkin Elmer, France) with an excitation wavelength of 485 nm and an emission wavelength of 535 nm.

### 4.9. Human topoisomerase I inhibition assay

The human DNA topoisomerase I inhibitory activity was determined by measuring the relaxation of supercoiled plasmid DNA pBR322. Each reaction mixture contained 10 mM Tris–HCl, pH 7.5, 100 mM NaCl, 1 mM phenylmethylsulfonyl fluoride, α-toluenesulfonyl fluoride, PMSF, and 1 mM 2-mercaptoethanol, 0.25 μg plasmid DNA pBR322, 1 unit of human DNA topoisomerase I, and the test compound at a specified concentration. The total volume of each reaction mixture was 20 μL and these mixtures were prepared on ice. Upon enzyme addition, reaction mixtures were incubated at 37 °C for 30 min. The reactions were terminated by the addition of

2 μL of 10% SDS, and then followed by 3 μL of dye solution comprising 0.02% bromophenol blue and 50% glycerol. SDS is required to denature topoisomerase I, preventing further functional enzymatic activity. Each mixture was applied to 1.2% agarose gel and underwent electrophoresis for 5 h at 33 V with running buffer of Tris–acetate EDTA, TAE. The gel was stained, destained and photographed under UV light using a Syngene Bio Imaging system and the digital image was viewed with Gene Flash software.

## Acknowledgements

The authors thank Peruntukan Penyelidikan Pascasiswazah (PPP, University of Malaya; PV036-2011A) and the Ministry of Higher Education of Malaysia (UM.C/HIR-MOHE/SC/12) for funding studies in metal-based drugs.

## Appendix A. Supplementary data

Supplementary data related to this article can be found at http://dx.doi.org/10.1016/j.ejmech.2013.06.038.

## References

[1] H. Wagner Jr., D.R. Parkinson, H. Madoc-Jones, E.S. Sternick, K. Vrusho, F. Krasin, Int. J. Rad. Oncol. Biol. Phys. 10 (1984) 1575–1579.
[2] T.S. Ying, D.S.R. Sarma, E. Farber, Am. J. Pathol. 99 (1980) 159–173.
[3] F.W. Sunderman, Ann. Clin. Lab. Sci. 9 (1979) 1–10.
[4] T.K. Schmalbach, R.F. Borch, Cancer Res. 49 (1989) 6629–6633.
[5] G. Hogarth, Mini-Rev. Med. Chem. 12 (2012) 1202–1215.
[6] E.R.T. Tiekink, Appl. Organomet. Chem. 22 (2008) 533–550.
[7] H. Li, C.S. Lai, J. Wu, P.C. Ho, D. de Vos, E.R.T. Tiekink, J. Inorg. Biochem. 101 (2007) 809–816.
[8] E.M. Nagy, S. Sitran, M. Montopoli, M. Favaro, L. Marchiò, L. Caparrotta, D. Fregona, J. Inorg. Biochem. 117 (2012) 131–139.
[9] Z. Skrott, B. Cvek, Mini-Rev. Med. Chem. 12 (2012) 1184–1192.
[10] E.R.T. Tiekink, Crit. Rev. Hematol. Oncol. 42 (2002) 225–245.
[11] E.R.T. Tiekink, Inflammopharmacology 16 (2008) 138–142.
[12] S.J. Berners-Price, A. Filipovska, Metallomics 3 (2011) 863–873.
[13] D. de Vos, S.Y. Ho, E.R.T. Tiekink, Bioinorg. Chem. Appl. 2 (2004) 141–154.
[14] A. Casini, G. Kelter, C. Gabbiani, M.A. Cinellu, G. Minghetti, D. Fregona, H.-H. Fiebig, L. Messori, J. Biol. Inorg. Chem. 14 (2009) 1139–1149.
[15] X. Zhang, M. Frezza, V. Milacic, L. Ronconi, Y. Fan, C. Bi, D. Fregona, Q.P. Dou, J. Cell. Biochem. 109 (2010) 162–172.
[16] L. Cattaruzza, D. Fregona, M. Mongiat, L. Ronconi, A. Fassina, A. Colombatti, D. Aldinucci, Int. J. Cancer 128 (2011) 206–215.
[17] M.N. Kouodom, G. Boscutti, M. Celegato, M. Crisma, S. Sitran, D. Aldinucci, F. Formaggio, L. Ronconi, D. Fregona, J. Inorg. Biochem. 117 (2012) 248–260.
[18] Z.U. Rahman, D.K. Frye, T.L. Smith, L. Asmar, R.L. Theriault, A.U. Buzdar, G.N. Hortobagyi, Cancer 85 (1999) 104–111.
[19] A.T. Brunetto, D. Sarker, D. Papadatos-Pastos, R. Fehrmann, S.B. Kaye, S. Johnston, M. Allen, J.S. De Bono, C. Swanton, Br. J. Cancer 103 (2010) 607–612.
[20] D.B. Longley, P.G. Johnston, J. Pathol. 205 (2005) 275–292.
[21] M.H. Andersen, J.C. Becker, P. Straten, Nat. Rev. Drug Discov. 4 (2005) 399–409.
[22] A.A. Stavrovskaya, Biochemistry 65 (2000) 95–106.
[23] M.M. Gottesman, Ann. Rev. Med. 53 (2002) 615–627.
[24] G.D. Kruh, Oncogene 22 (2003) 7262–7264.
[25] R. Krishna, L.D. Mayer, Eur. J. Pharmacol. Sci. 11 (2000) 265–283.
[26] S.V. Ambudkar, C. Kimchi-Sarfaty, Z.E. Sauna, M.M. Gottesman, Oncogene 22 (2003) 7468–7485.
[27] S. Malla, N.P. Niraula, K. Liou, J.K. Sohng, Res. Microbiol. 161 (2010) 109–117.
[28] B. Vincenzi, A.M. Frezza, D. Santini, G. Tonini, Expert Opin. Emerging Drugs 15 (2010) 237–248.
[29] C.W. Taylor, W.S. Dalton, P.R. Parrish, M.C. Gleason, W.T. Bellamy, F.H. Thompson, D.J. Roe, J.M. Trent, Br. J. Cancer 63 (1991) 923–929.
[30] S.Y. Ho, E.R.T. Tiekink, Acta Crystallogr. E57 (2001) m603–m604.
[31] S.Y. Ho, E.R.T. Tiekink, Z. Kristallogr. NCS 217 (2002) 359–360.
[32] S.Y. Ho, E.R.T. Tiekink, Z. Kristallogr. NCS 220 (2005) 342–344.
[33] J.G. Wijnhoven, W.P. Bosman, P.T. Beurskens, J. Cryst. Mol. Struct. 2 (1972) 7–15.
[34] M.G. Ormerod, M.K. Collins, G. Rodriguez-Tarduchy, D. Robertson, J. Immunol. Methods 153 (1992) 57–65.
[35] J. Kapuscinski, Z. Darzynkiewicz, M.R. Melamed, Biochem. Pharmacol. 32 (1983) 3679–3694.
[36] C.J.G. Yeh, B.L. Hsi, W.P. Faulk, J. Immunol. Methods 43 (1981) 269–275.
[37] C. Foglieni, C. Meoni, A.M. Davalli, Histochem. Cell Biol. 115 (2001) 223–229.
[38] S. Nagata, Ann. Rev. Immunol. 23 (2005) 853–875.
[39] K. Samejima, W.C. Earnshaw, Nat. Rev. Mol. Cell. Biol. 6 (2005) 677–688.
[40] A.H. Wyllie, J.F.K. Kerr, A.R. Currie, Int. Rev. Cytol. 68 (1980) 251–306.
[41] L.G. Koss, in: L.G. Koss (Ed.), Diagnostic Cytology and Its Histopathologic Bases, J.P. Lippincott & Co., Philadelphia, 1992, pp. 687–702.
[42] G. Kroemer, B. Dallaporta, M. Resche-Rigon, Ann. Rev. Physiol. 60 (1998) 619–642.
[43] M. Oren, C. Prives, Biochim. Biophys. Acta 1288 (1996) 13–19.
[44] B. Zhivotovsky, G. Kroemer, Nat. Rev. Mol. Cell Biol. 5 (2004) 752–762.
[45] S. Bouleau, I. Parvu-Ferecatu, A. Rodriguez-Enfedaque, V. Rincheval, H. Grimal, B. Mignotte, J.L. Vayssière, F. Renaud, Apoptosis 12 (2007) 1377–1387.
[46] M. Dobbelstein, S. Strano, J. Roth, G. Blandino, Biochem. Biophys. Res. Commun. 331 (2005) 688–693.
[47] P. Fei, W. Wang, S.H. Kim, S. Wang, T.F. Burns, J.K. Sax, M. Buzzai, D.T. Dicker, W.G. McKenna, E.J. Bernhard, W.S. El-Deiry, Cancer Cell 6 (2004) 597–609.
[48] J. Zhu, J. Jiang, W. Zhou, X. Chen, Cancer Res. 58 (1998) 5061–5065.
[49] H. Takahashi, S. Ichimiya, Y. Nimura, M. Watanabe, M. Furusato, S. Wakui, R. Yatani, S. Aizawa, A. Nakagawara, Cancer Res. 58 (1998) 2076–2077.
[50] S. Kovalev, N. Marchenko, S. Swendeman, M. LaQuaglia, U.M. Moll, Cell Growth Differ. 9 (1998) 897–903.
[51] M.S. Irwin, K. Kondo, M.C. Marin, L.S. Cheng, W.C. Hahn, W.G. Kaelin Jr., Cancer Cell 3 (2003) 403–410.
[52] G. Melino, V. De Laurenzi, K.H. Vousden, Nat. Rev. Cancer 2 (2002) 605–615.
[53] Y. Tsujimoto, S. Shimizu, FEBS Lett. 466 (2000) 6–10.
[54] R. Eskes, B. Antonsson, A. Osen-Sand, S. Montessuit, C. Richter, R. Sadoul, G. Mazzei, A. Nichols, J.C. Martinou, J. Cell Biol. 143 (1998) 217–224.
[55] A. Gross, J.M. McDonnell, S.J. Korsmeyer, Genes Dev. 13 (1999) 1899–1911.
[56] G. Melino, F. Bernassola, M. Ranalli, K. Yee, W.X. Zong, M. Corazzari, R.A. Knight, D.R. Green, C. Thompson, K.H. Vousden, J. Biol. Chem. 279 (2004) 8076–8083.
[57] P.X. Petit, S.A. Susin, N. Zamzami, B. Mignotte, G. Kroemer, FEBS Lett. 396 (1996) 7–13.
[58] G. Kroemer, L. Galluzzi, C. Brenner, Physiol. Rev. 87 (2007) 99–163.
[59] L.Y. Li, X. Luo, X. Wang, Nature 412 (2001) 95–99.
[60] G. van Loo, P. Schotte, M. van Gurp, H. Demol, B. Hoorelbeke, K. Gevaert, I. Rodriguez, A. Ruiz-Carrillo, J. Vandekerckhove, W. Declercq, R. Beyaert, P. Vandenabeele, Cell Death Differ. 8 (2001) 1136–1142.
[61] A. Thorburn, Cell. Signal. 16 (2004) 139–144.
[62] R.M.A. El-Ghany, N.M. Sharaf, L.A. Kassem, L.G. Mahran, O.A. Heikal, Drug Discov. Ther. 3 (2009) 296–306.
[63] H. Walczak, P.H. Krammer, Exp. Cell Res. 256 (2000) 58–66.
[64] P.H. Krammer, Nature 407 (2000) 789–795.
[65] D. Milhas, O. Cuvillier, N. Therville, P. Clavé, M. Thomsen, T. Levade, H. Benoist, B. Ségui, J. Biol. Chem. 280 (2005) 19836–19842.
[66] S. Fulda, Cancer Lett. 281 (2009) 128–133.
[67] X.M. Yin, Gene 369 (2006) 7–19.
[68] C.P. LeBel, H. Ischiropoulos, S.C. Bondy, Chem. Res. Toxicol. 5 (1992) 227–231.
[69] A. Gomes, E. Fernandes, J.L. Lima, J. Biochem. Biophys. Methods 65 (2005) 45–80.
[70] V.P. Skulachev, FEBS Lett. 397 (1996) 7–10.
[71] M. Le Bras, M.V. Clément, S. Pervaiz, C. Brenner, Histol. Histopathol. 20 (2005) 205–219.
[72] F. Chen, V. Vallyathan, V. Castranova, X. Shi, Mol. Cell. Biochem. 222 (2001) 183–188.
[73] P.H. Krammer, Adv. Immunol. 71 (1999) 163–210.
[74] G.M. Ledda-Columbano, P. Coni, M. Curto, L. Giacomini, G. Faa, S. Oliverio, M. Piacentini, A. Columbano, Am. J. Pathol. 139 (1991) 1099–1109.
[75] J.S. Sun, Y.H. Tsuang, W.C. Huang, L.T. Chen, Y.S. Hang, F.T. Lu, Cell. Mol. Life Sci. 53 (1997) 967–976.
[76] B.F. Trump, P.J. Goldblatt, R.E. Stowell, Lab. Invest. 14 (1965) 2000–2028.
[77] C.O. Bellamy, R.D. Malcomson, D.J. Harrison, A.H. Wyllie, Semin. Cancer Biol. 6 (1995) 3–16.
[78] C. Richter, M. Schweizer, A. Cossarizza, C. Franceschi, FEBS Lett. 378 (1996) 107–110.
[79] M. Leist, B. Single, A.F. Castoldi, S. Kuhnle, P. Nicotera, J. Exp. Med. 185 (1997) 1481–1486.
[80] Y. Eguchi, S. Shimizu, Y. Tsujimoto, Cancer Res. 57 (1997) 1835–1840.
[81] C.S. Nobel, D.H. Burgess, B. Zhivotovsky, M.J. Burkitt, S. Orrenius, A.F. Slater, Chem. Res. Toxicol. 10 (1997) 636–643.
[82] M.B. Hampton, S. Orrenius, FEBS Lett. 414 (1997) 552–556.
[83] B. Levine, D.J. Klionsky, Dev. Cell 6 (2004) 463–477.
[84] S. Bialik, A. Kimchi, Ann. Rev. Biochem. 75 (2006) 189–210.
[85] J.C. Kuo, W.J. Wang, C.C. Yao, P.R. Wu, R.H. Chen, J. Cell Biol. 172 (2006) 619–631.
[86] B. Harrison, M. Kraus, L. Burch, C. Stevens, A. Craig, P. Gordon-Weeks, T.R. Hupp, J. Biol. Chem. 283 (2008) 9999–10014.
[87] H.J. Yoo, H.J. Byun, B.R. Kim, K.H. Lee, S.Y. Park, S.B. Rho, Cell Signal. 24 (2012) 1471–1477.
[88] L. Yang, Z. Cao, H. Yan, W.C. Wood, Cancer Res. 63 (2003) 6815–6824.
[89] L. Eckhart, H. Fischer, E. Tschachler, Biochem. Biophys. Res. Commun. 356 (2007) 293–299.
[90] J.J. Champoux, Ann. Rev. Biochem. 70 (2001) 369–413.
[91] J.C. Wang, Ann. Rev. Biochem. 65 (1996) 635–692.
[92] D.A. Burden, N. Osheroff, Biochim. Biophys. Acta 1400 (1998) 139–154.

[93] A.K. Larsen, A.E. Escargueil, A. Skladanowski, Pharmacol. Ther. 99 (2003) 167–181.
[94] Y. Pommier, Nat. Rev. Cancer 6 (2006) 789–802.
[95] S. Sunami, T. Nishimura, I. Nishimura, S. Ito, H. Arakawa, M. Ohkubo, J. Med. Chem. 52 (2009) 3225–3237.
[96] B.A. Teicher, Biochem. Pharmacol. 75 (2008) 1262–1271.
[97] G.L. Beretta, P. Perego, F. Zunino, Expert Opin. Ther. Targets 12 (2008) 1243–1256.
[98] C.I. Yeo, K.K. Ooi, A. Md Akim, K.P. Ang, Z.A. Fairuz, Siti N.B.A. Halim, S.W. Ng, H.-L. Seng, E.R.T. Tiekink, J. Inorg. Biochem., 2013. http://dx.doi.org/10.1016/j.jinorgbio.2013.05.011.
[99] CrysAlis PRO, Agilent Technologies, Yarnton, Oxfordshire, England, 2011.
[100] G.M. Sheldrick, Acta Crystallogr. Sect. A 64 (2008) 112–122.
[101] L.J. Farrugia, J. Appl. Crystallogr. 45 (2012) 849–854.
[102] J. Gans, D. Shalloway, J. Mol. Graphics Modell. 19 (2001) 557.
[103] K. Brandenburg, DIAMOND, Crystal Impact GbR, Bonn, Germany, 2006.